Constructional Volcanic Edifices on Mercury: Candidates and Hypotheses of Formation

Journal of Geophysical Research: Planets

RESEARCH ARTICLE
10.1002/2017JE005450

Key Points:
- We report two peak-like landforms that may be small volcanic constructs
- These edifices resemble Earth and Moon volcanoes, but we cannot exclude alternative formation hypotheses with MESSENGER data
- Data from the BepiColombo mission should be used to test the volcanic interpretations for these candidate edifices and search for others

Supporting Information:
- Supporting Information S1

Correspondence to:
J. Wright,
jack.wright@open.ac.uk

Citation:
Wright, J., Rothery, D. A., Balme, M. R., & Conway, S. J. (2018). Constructional volcanic edifices on Mercury: Candidates and hypotheses of formation. *Journal of Geophysical Research: Planets*, *123*, 952–971. https://doi.org/10.1002/2017JE005450

Received 15 SEP 2017
Accepted 13 MAR 2018
Accepted article online 25 MAR 2018
Published online 16 APR 2018

Constructional Volcanic Edifices on Mercury: Candidates and Hypotheses of Formation

Jack Wright[1], David A. Rothery[1], Matthew R. Balme[1], and Susan J. Conway[2]

[1]School of Physical Sciences, Open University, Milton Keynes, UK, [2]CNRS, Laboratoire de Planétologie et Géodynamique, Université de Nantes, Nantes, France

Abstract Mercury, a planet with a predominantly volcanic crust, has perplexingly few, if any, constructional volcanic edifices, despite their common occurrence on other solar system bodies with volcanic histories. Using image and topographical data from the MErcury Surface, Space ENvironment, GEochemistry, and Ranging (MESSENGER) spacecraft, we describe two small (<15-km diameter) prominences with shallow summit depressions associated with volcanically flooded impact features. We offer both volcanic and impact-related interpretations for their formation, and then compare these landforms with volcanic features on Earth and the Moon. Though we cannot definitively conclude that these landforms are volcanic, the paucity of constructional volcanic edifices on Mercury is intriguing in itself. We suggest that this lack is because volcanic eruptions with sufficiently low eruption volumes, rates, and flow lengths, suitable for edifice construction, were highly spatiotemporally restricted during Mercury's geological history. We suggest that volcanic edifices may preferentially occur in association with late-stage, postimpact effusive volcanic deposits. The European Space Agency/Japan Aerospace Exploration Agency BepiColombo mission to Mercury will be able to investigate further our candidate volcanic edifices; search for other, as-yet unrecognized edifices beneath the detection limits of MESSENGER data; and test our hypothesis that edifice construction is favored by late-stage, low-volume effusive eruptions.

Plain Language Summary MErcury Surface, Space ENvironment, GEochemistry, and Ranging (MESSENGER) data show that most of Mercury's surface consists of lava plains. However, no volcanoes (mountains built by eruptions) have been found to date. This is unexpected because planets and moons with lava plains also have volcanoes. We conducted a new search and found two good candidate volcanoes. We cannot be sure that they are volcanoes based on MESSENGER data. Nevertheless, the observation that volcanoes on Mercury are rare is important itself. It means most eruptions on Mercury were somehow different from those that made volcanoes elsewhere in the solar system. We suggest that most eruptions on Mercury were too large and rapid, meaning that lava spread out to form plains, rather than building volcanoes. We suggest that eruptions small enough to build volcanoes might have occurred in Mercury's later history, when it was cooler and less able to generate magma. Impact craters may have helped later magma to erupt by opening fractures in Mercury's crust. We suggest that BepiColombo, the next spacecraft mission to Mercury, should target impact craters to find more volcanoes and return better observations of our candidates.

1. Introduction

Constructional volcanic edifices, which form from the accumulation of erupted products proximal to their vent (Davidson & de Silva, 2000), have been recognized throughout the solar system (Sigurdsson et al., 2000) but have not been positively identified on Mercury. The morphology of volcanic landforms reflects the style and environment of eruption, which in turn provides insight into interior processes of planetary bodies. Therefore, characterizing the full range of volcanic landforms and their spatiotemporal distributions is required to understand the geological evolution of the body on which they occur. Here we describe previously recognized volcanic morphologies on Mercury, before introducing two candidate constructional volcanic edifices we have identified.

1.1. Smooth Plains Volcanism

Mercury has abundant smooth plains, first imaged by Mariner 10, most of which are interpreted as effusive lava plains (Head et al., 2008; Strom et al., 1975). More recent imaging by the MErcury Surface, Space

ENvironment, GEochemisty, and Ranging (MESSENGER) spacecraft shows that smooth plains cover ~27% of the planet's surface (Denevi et al., 2013) and suggests that Mercury's intercrater plains are older, more heavily cratered lava plains (Whitten et al., 2014), indicating that the planet's crust is predominantly volcanic. This volcanic style is analogous to large igneous provinces (LIPs) on Earth, which have high erupted volumes that form thick plains (Bryan & Ernst, 2008). The most extensive smooth plains on Mercury are those constituting Borealis Planitia (informally the "northern smooth plains"; Head et al., 2011; Ostrach et al., 2015) and those smooth plains associated with the Caloris impact basin. The plains interior to the basin are formally "Caloris Planitia" (Strom et al., 1975), and the plains surrounding Caloris have been informally referred to as the "circum-Caloris" plains (Denevi et al., 2013; Fassett et al., 2009). Observations of the relationships between Caloris Planitia and the circum-Caloris smooth plains (Rothery et al., 2017) and their superposing crater densities (Denevi et al., 2013; Fassett et al., 2009; Ostrach et al., 2015) suggest that they formed within a short span of geological time. Absolute ages on Mercury have intrinsically large errors due to the uncertainties in the crater production function used to derive them (e.g., Le Feuvre & Wieczorek, 2011; Marchi et al., 2009; Neukum et al., 2001; Strom & Neukum, 1988). However, both Borealis and Caloris Planitia, and the circum-Caloris plains, are estimated to have formed ~3.7 Ga (Denevi et al., 2013; Head et al., 2011; Ostrach et al., 2015), and large-scale effusive volcanism is believed to have ceased soon after (i.e., ~3.5 Ga; Byrne et al., 2016).

1.2. Explosive Volcanism

MESSENGER also identified bright, spectrally red spots with diffuse outer boundaries, usually with an irregular depression in their centers. These are interpreted as pyroclastic deposits surrounding explosively excavated volcanic craters (Goudge et al., 2014; Head et al., 2008; Jozwiak et al., 2018; Kerber et al., 2009, 2011; Murchie et al., 2008; Thomas et al., 2014c). The oldest pyroclastic deposit dated using crater counting by Thomas et al. (2014b) was determined to have formed ~3.9 Ga, and explosive volcanism of this kind appears to have been active until at least ~1.0 Ga (Jozwiak et al., 2018; Thomas et al., 2014b).

1.3. A Shield Volcano?

A candidate shield volcano was proposed within Caloris Planitia based on images captured during MESSENGER's first flyby (Head et al., 2008). Shield volcanoes form by eruptions of low-viscosity lavas from a point source, along with a relatively minor pyroclastic component and, in addition to those on Earth, have been reported on the Moon, Venus, Mars, and Io (Sigurdsson et al., 2000). Shield volcanism represents an end-member eruptive style that brackets a continuum with LIPs (Greeley, 1982). Evidence for the shield volcano in Caloris Planitia included apparent embayment of nearby impact craters and an albedo change surrounding a "kidney-shaped depression" (Head et al., 2008). However, subsequent orbital data cast doubt on the shield interpretation of this edifice. Higher-resolution images captured under a range of illumination conditions show that impact craters proximal to the Caloris depression are not obviously embayed by flows (Rothery et al., 2014). Furthermore, detrended Mercury Laser Altimeter (MLA; Cavanaugh et al., 2007) data (where long-wavelength slopes are removed from local topography) show that although the excavated depression, regarded as a vent, is more than 1 km deep, its brink is not substantially elevated above its surroundings, and the external flank slopes of the candidate "shield" are ~0.14° (Rothery et al., 2014). This slope value is even lower than those typical for low shields on Mars (0.43°; Hauber et al., 2009) and at the lowermost bound of the extremely low-angle shields that have been identified on that planet (0.15–0.35°; Vaucher et al., 2009). Martian shields have some of the lowest flank slopes in the solar system, suggesting that the low topographic rise around the Caloris vent could have been constructed by other means. A study that considered 20 additional explosive vents on Mercury, situated on otherwise generally flat plains, found that six of these are associated with little ($<1°$) or no relief (Thomas et al., 2014c). Therefore, these landforms more likely represent subtle ramps generated by the ballistic emplacement of pyroclasts from the explosive eruption of a compound volcanic vent, rather than a true shield constructed predominantly of lava flows (Rothery et al., 2014).

These findings suggest that explosive volcanism on Mercury has been chiefly excavational in nature, producing large craters and thin deposits morphologically resembling those of maar volcanoes (White & Ross, 2011) or phreatic explosions (Browne & Lawless, 2001). Examples of constructional volcanic edifices, where the landform is characterized by a topographic rise, rather than a large crater (Davidson & de Silva, 2000), have hitherto not been observed on Mercury, despite extensive study with orbital MESSENGER observations of Borealis Planitia (Byrne et al., 2013; Head et al., 2011; Ostrach et al., 2015), the Caloris plains (Denevi et al., 2013), and intercrater plains (Whitten et al., 2014).

1.4. Constructing Volcanic Edifices

Given the lack of erosional processes that could fully remove evidence of volcanic edifices in the smooth plains, their paucity suggests that Mercury's volcanic eruptions during its early history (>3.5 Ga; Byrne et al., 2016) were somehow unable to build substantial topography. This has been attributed to the planet's erupted lavas having very low viscosities (Stockstill-Cahill et al., 2012). Streamlined kipukas and eroded lava channels provide evidence that the widespread smooth plains of Mercury were emplaced at least partly by "voluminous, high-temperature, low-viscosity lavas of mafic to ultramafic composition" (Byrne et al., 2013). However, the typical viscosity of Mercury's lavas is predicted to have increased through time. Decreasing eruption temperatures and degrees of partial melting will have occurred as secular cooling of the planet's interior progressed, forming melts with higher crystal fractions, silica content, and consequently higher viscosities (Namur & Charlier, 2017). This suggests that late-stage eruptions may have been more capable than earlier ones of constructing edifices.

Lava viscosity is not the only control on edifice construction. For a given lava viscosity, construction capacity increases with decreasing effusion rate, erupted volume, and flow length, as demonstrated on Earth by the Galápagos shields. These have a break in slope between low-slope flank eruptions and steeper summit eruptions, giving them an "inverted soup dish" shape, compared with the uniformly shallow flanked Hawaiian shields (Naumann & Geist, 2000). Since edifice construction on Earth is associated with lower erupted volumes than LIPs in general (Bryan & Ernst, 2008), identifying sites of low-volume effusive volcanism on Mercury may be the key to discovering constructional volcanic edifices on its surface.

Here we describe two small (i.e., <15 km in diameter) positive-relief features with summit depressions that are plausibly of volcanic origin. These features were discovered serendipitously but, following a global search of the smooth plains, which represent the last effusions of lava, we found no additional similar features. We regard it as unlikely that any stronger candidate constructional volcanic edifices remain undetected in the MESSENGER data. We compare the morphologies and settings of the candidate volcanic edifices to volcanoes on Earth and the Moon and discuss their possible origin(s), volcanic or otherwise.

2. Data and Methods

We searched for volcanic edifices using the ~166-m/pixel monochrome Mercury Dual Imaging System (MDIS) global mosaic (Chabot et al., 2016; Hawkins et al., 2007). Where available, we inspected higher-resolution narrow-angle camera (NAC) and wide-angle camera (WAC) images and MLA topographic profiles across candidate volcanic edifices. We made color observations using ~665-m/pixel enhanced color global mosaic and RGB-combined WAC images. We used the Integrated Software for Imagers and Spectrometers package of the U.S. Geological Survey to perform standard radiometric and photometric corrections on the NAC and WAC products. RGB-combined mosaics were made using 1,000, 750, and 430-nm WAC narrow band filter images in the red, green, and blue channels, respectively (Denevi et al., 2016; Hawkins et al., 2007). The enhanced color mosaic also uses the 1,000, 750, and 430-nm WAC bands and places the second principal component, the first principal component, and the 430/1,000 ratio in the red, green, and blue channels, respectively (Denevi et al., 2009, 2016). These products were then map projected into individual sinusoidal projections with central meridians running through their respective geographic centers. We used the 665-m/pixel global stereo digital elevation model (DEM) of Mercury by Becker et al. (2016) to investigate the topography of regions of interest, although this data set has insufficient resolution to characterize features <15 km across well. We analyzed these data using ESRI ArcMap 10.1 geographic information system software.

We measured the diameters of our candidate volcanoes using CraterTools (Kneissl et al., 2011), which minimizes projection-related errors when measuring distances. The diameters were calculated from circles we fitted to the candidate volcanoes using the 3-point method within CraterTools (Kneissl et al., 2011). We measured the height of candidate volcano #1 ("CV1") using shadow-length calculations (Barnouin et al., 2012). We also derived a profile of CV1 using its shadow shape by employing the method of Basilevsky (2002). To do this, we scaled down the image of CV1 in which it casts a shadow on a flat surface in the direction of the solar azimuth by a scale factor given by

$$\tan i \pm \tan e, \tag{1}$$

where i and e are the solar incidence and spacecraft emission angles, respectively. In the scaled image, the distance to the umbral shadow of the candidate cast on a flat surface measured from a point on the terminator of the landform in the direction of the solar azimuth returns the elevation at that point.

Mercury Laser Altimeter data were available to measure the shape of candidate volcano #2. Following the method used by Kreslavsky and Head (1999), we calculated the point-to-point slopes along the MLA track coincident with the landform. We discarded point-to-point slopes when along-profile spacing between the MLA points was more than the normal consecutive shot separation of ~500 m. The calculated flank slope of the landform is the median of the retained point-to-point slopes.

For our comparison with Earth volcanoes, we used ESRI World imagery and the Advanced Spaceborne Thermal Emission and Reflection (ASTER) Global Digital Elevation Map V0002. For the Moon, we used the global Lunar Reconnaissance Orbiter Camera (LROC) WAC 100-m/pixel mosaic, individual LROC NAC frames, and the global Lunar Orbiter Laser Altimeter (LOLA) 118-m/pixel DEM (Chin et al., 2007; M. S. Robinson et al., 2010; Smith et al., 2010). The full list of data products used in this paper is given as supporting information.

3. Results and Interpretations

3.1. Candidate Volcano #1

3.1.1. Observations

Candidate volcano #1 ("CV1") is a positive-relief feature situated within the Heaney impact crater (diameter ~125 km, Figure 1a), at 123°02′14″E, 34°07′40″S. CV1 is approximately circular in plan view (Figure 1b) and has a basal diameter of 6.1 km, a height of ~530 m (from shadow calculations), and flank slopes of ~10° (treating it as a simple cone). It is the highest topographic prominence within Heaney and is located 30.5 km from the crater's center. There is a bowl-shaped depression, 1.7 km across, at the summit of CV1, with a separate depression running up from the base of the northern flank. Based on shadow calculations, the summit depression has a depth-diameter (d/D_{rim}) ratio of 0.14, which is shallower than the d/D_{rim} ratio (0.19) of the fresh impact crater indicated in Figure 1b (see also Fassett et al., 2017). The ratio of the summit depression diameter to the basal diameter of CV1 is ~0.28. It is unclear in any available NAC image whether the summit depression is younger or older than the flank depression. To the west, there are two much smaller knobs that form a straight line with the landform. In enhanced color (Figures 1c and 1d), CV1 is surrounded by a diffuse, red color anomaly, whereas impact craters nearby with visible ejecta have blue color signatures. The smaller knobs have no visible color anomalies.

Smooth plains with small wrinkle ridges cover the floor of Heaney (Figures 1a and 2a), subduing the topographic range within the crater (Figure 2b) compared to craters of this size without smooth plains. There is no evidence that smooth plains material cascaded into the crater from the surroundings. The unburied crater rim is relatively crisp, and the continuous ejecta blanket extends radially by about one crater diameter beyond the rim, superposing external smooth plains nearby. The present-day depth of the crater, measured using the global stereo DEM (Becker et al., 2016), and defined as maximum rim elevation minus minimum floor elevation (ignoring superposing impact craters), is ~3,500 m.

Impact craters on Mercury of the same diameter as Heaney can have a variety of morphologies (Figure 3). Complex craters (50–168 km) have central peaks, peak-ring basins (84–320 km) have a ring of peaks, and protobasins (50–195 km) have both a central peak and ring of peaks (Baker & Head, 2013). The present maximum depth of Heaney (3,500 m) offers some constraint on the crater's original morphology, now obscured by the smooth plains. Baker and Head (2013) showed that the mean depth-diameter (d/D_{rim}) ratio of complex craters on Mercury (0.034 ± 0.010) is greater than that of protobasins (0.027 ± 0.007), which in turn have a greater mean d/D_{rim} ratio than that of peak-ring basins (0.017 ± 0.006). Using these values and the diameter of Heaney (125 km), its predicted original depth range is 3,000–5,500 m for a complex crater, 2,500–4,250 m for a protobasin, and 2,050–2,200 m for a peak-ring basin. This suggests that Heaney is too deep to have formed as a peak-ring basin, but it could be a partially infilled protobasin or complex crater. Estimates for maximum thicknesses of the smooth plains in Heaney are 750 and 2,000 m for protobasin and complex crater morphologies, respectively.

In enhanced color, Heaney crater appears to have exhumed dark blue, low-reflectance material (LRM; Robinson et al., 2008) in its southern rim and ejecta (Figure 1c), whereas its smooth fill corresponds to the surface unit termed low-reflectance blue plains by Denevi et al. (2009). The crater rim is generally blue but appears somewhat redder in the northeast.

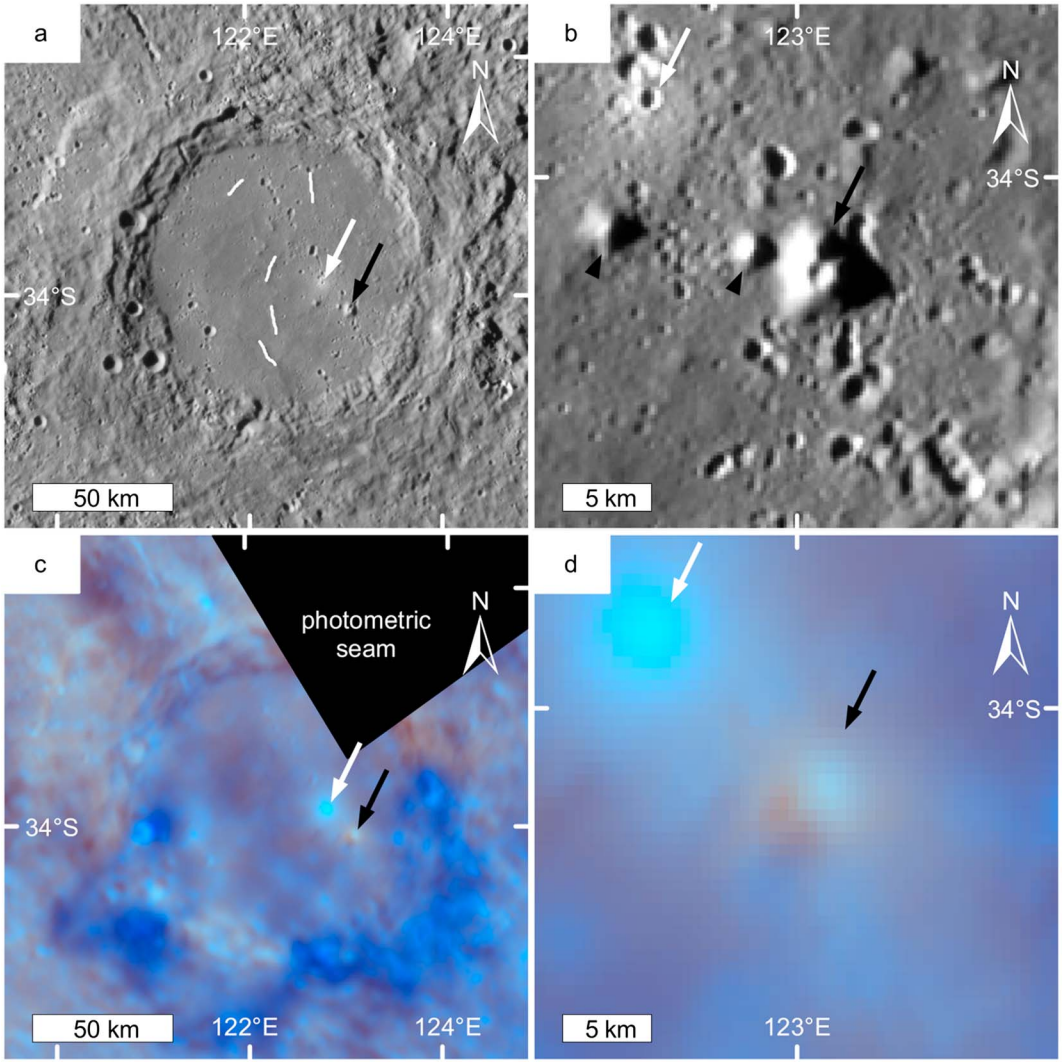

Figure 1. Photogeological and color observations of candidate volcano #1 (CV1). CV1 is indicated with a black arrow, and a nearby, young impact crater is indicated with a white arrow. (a) Location of CV1 within Heaney, a young impact crater nearby, and small wrinkle ridges within the smooth infill (white lines). (b) Detail of CV1, the young impact crater, and small knobs nearby (black triangles) (MDIS image EN0251749039M). (c) Enhanced color view of Heaney crater. The red color anomaly associated with CV1. The high-albedo blue color anomaly associated with the young impact crater. A portion of the mosaic in the upper-right corner of the figure has been masked out due to a photometric seam. (d) Detail of the color anomalies of CV1 and the young impact crater.

Next, we discuss potential explanations for these observations as a result of either impact or volcanic processes.

3.1.2. Impact Interpretation

An initial hypothesis for the formation of CV1 is that it is part of Heaney's peak-ring. The relatively undegraded state of the crater and its ejecta superposing smooth plains nearby suggest a late-Calorian/early-Mansurian age for the impact (Kinczyk et al., 2016). The base of the Mansurian is conventionally held to be ~3.5–3.0 Ga (Spudis & Guest, 1988), although a recent study has revised the base to ~1.7 Ga (Banks et al., 2017). In any case, widespread effusive volcanism is thought to have ceased long before the Mansurian (Byrne et al., 2016). A crater in this degradation state would ordinarily be expected to host a preserved central peak or peak-ring (Kinczyk et al., 2016). If CV1 were a remnant peak-ring element, then its summit depression would be merely a coincidentally superposed impact crater. The northern flank depression can be interpreted as part of a secondary crater chain, of which the summit depression may also be a part. The summit depression's shallow appearance compared with primary impact craters of similar diameter on the

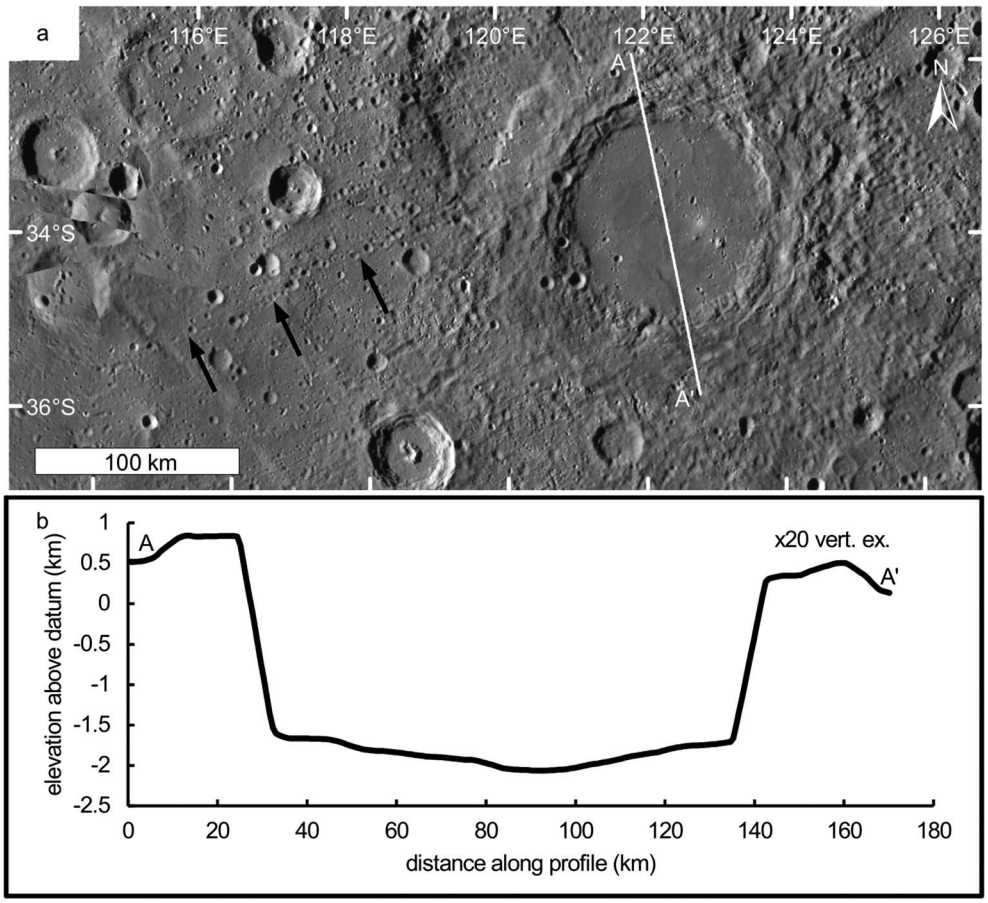

Figure 2. Observations of Heaney crater. (a) Geological setting of the crater. Heaney has a textured ejecta blanket that extends beyond its rim by approximately one crater diameter. The black arrows indicate a secondary crater chain attributable to Heaney that superposes nearby smooth plains. The line marked *A*-*A*′ represents the cross section shown in b. (b) The topography of Heaney measured from the global stereo digital elevation model of Mercury (Becker et al., 2016). The elevation of the smooth plains monotonically decreases toward the center of the crater and gives no obvious indication of the presence of any internal uplift (central peak or peak-ring).

surrounding smooth plains could be due to it being a secondary crater, since these exhibit atypical morphometries compared with primary craters (Strom et al., 2008). In addition, the shallowness of the depression might be due to its formation at the apex of a cone, since topographic slopes have been shown to affect impact crater depth (Aschauer & Kenkmann, 2017). If the summit depression is an impact crater, the red color anomaly associated with the landform could be due to its ejecta. The smaller knobs to the west of the feature could be other peak-ring elements appearing just above the subsequent infill. The burial of the rest of the presumably once-present peak-ring suggests that the smooth infill is due to thick volcanic flooding, rather than merely the volume of impact melt originally produced (Cintala & Grieve, 1998; Grieve & Cintala, 1992). Postimpact volcanism of this kind is a widespread process that is well documented on Mercury (Prockter et al., 2010; Strom et al., 1975). Originally, the smooth plains probably had a flat surface, but this will have subsided in the center, where the fill was originally thickest, producing the concave-up topography within the present-day crater interior (Blair et al., 2013).

We tested this remnant peak-ring element hypothesis by using the empirical relation between crater rim diameter, D_{rim}, and peak-ring diameter, D_{ring}, found by Baker et al. (2011) to be given by the relation

$$D_{ring} = AD_{rim}^{p} \quad (2)$$

The values of A and p are empirical constraints that are different for peak-ring basins and protobasins and are given in Table 2 of Baker et al. (2011). Given Heaney's rim diameter of 125 km, its peak-ring radius is predicted

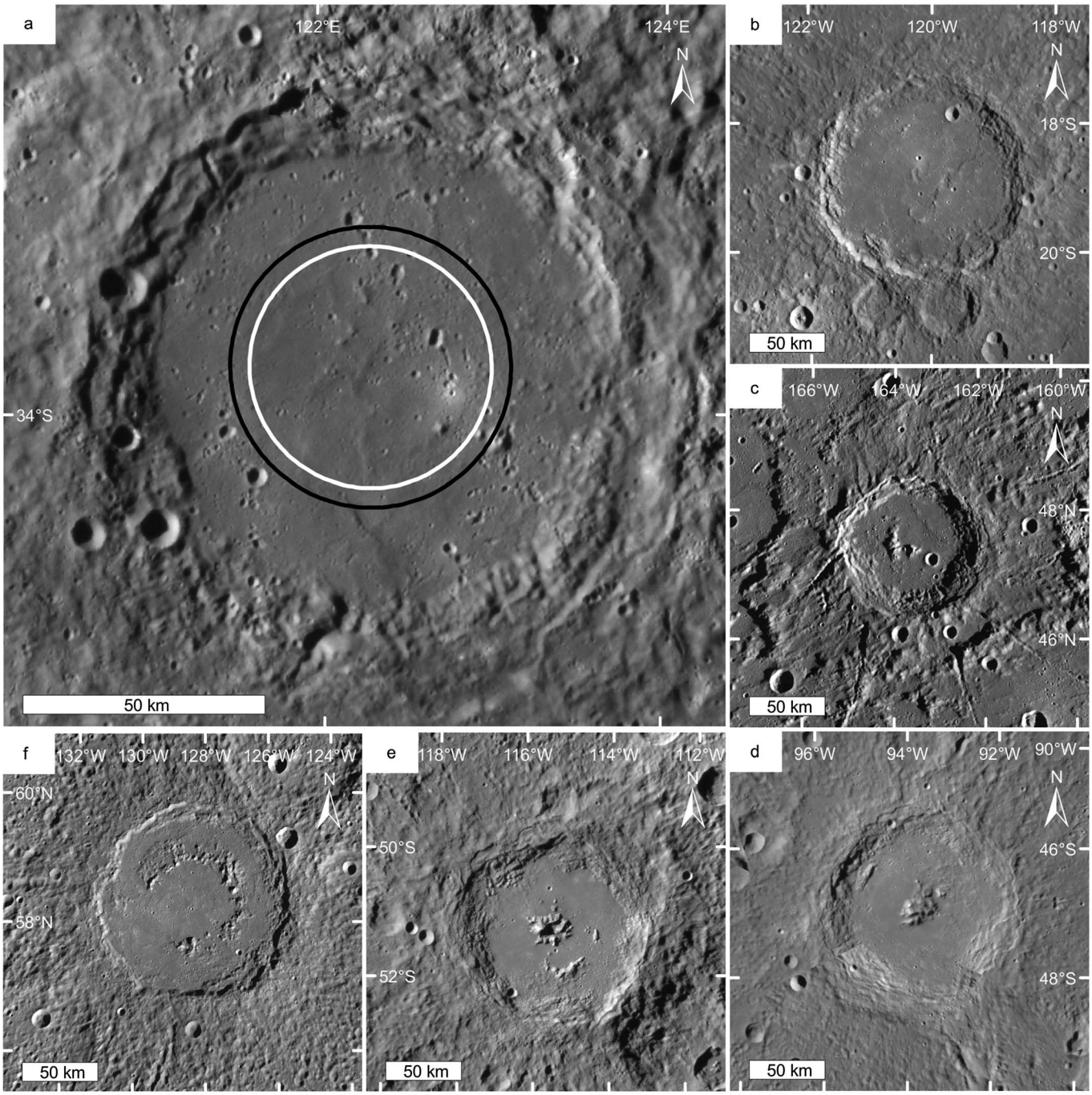

Figure 3. Comparison of Heaney with other impact features on Mercury that are similar in age and size. (a) Heaney. The circles represent expected radii of peak-rings for a peak-ring basin (black) and protobasin (white) of similar diameter to Heaney, per equation (2). Note that the other small knobs in Heaney do not lie where one would expect to find the highest peak elements. (b) Bello (diameter 139 km) located within Beethoven. Bello has a very similar size, apparent morphology, and degradation state to Heaney. Smooth plains, of probable volcanic origin, obscure any internal peaks that may have been present. (c) Mansur (diameter 95 km), the degradation state of which defines the base of the Mansurian time system on Mercury. Heaney has a similar degradation state, suggesting that it formed at a similar time. (d) Sūr Dās (diameter 131 km) with a central peak rather than a peak-ring. It is therefore possible that Heaney originally had no peak-ring. (e) Hawthorne (diameter 120 km), a protobasin. (f) Ahmad Baba (diameter 126 km), a peak-ring basin.

by this relation to be ~29 or ~25 km for a peak-ring or protobasin morphology, respectively. Therefore, CV1 is at a radial distance from Heaney's center (30.5 km) more consistent with the crater being a flooded peak-ring basin than a protobasin.

However, the remnant peak-ring element interpretation is not well supported. As stated previously, our measurements show that Heaney is very deep for it to be an infilled peak-ring basin. Furthermore, it is unclear why the rest of the presumed peak-ring is buried by smooth plains material with no clear surface expression, when CV1 has 530 m of relief. Measurements of the heights of peak-rings on Mercury suggest it is unlikely that the range of peak element heights in undegraded basins is greater than 500 m (Baker & Head, 2013). This seems to require (1) CV1 to be exceptionally tall compared with the rest of the peak-ring, allowing it to have escaped burial; (2) extreme differential erosion of the peak-ring; or (3) the peak-ring to have been highly incomplete when it formed.

The crater Bello, of comparable diameter, depth, degradation state, and, we therefore interpret, age, also has a floor covered by smooth plains, leaving no trace of any central peak or peak-ring that might once have been present (Figure 3b). This suggests that the floors and peaks of both Heaney and Bello are deeply buried. CV1 is situated toward Heaney's crater wall, where the fill is likely to be thinnest, yet even the immediately adjacent peak elements that we might expect to be present do not manifest. It seems unlikely that the rest of any peak-ring is buried just beneath the surface, as the wrinkle ridges within the fill do not form a ring marking its expected location as they can do with buried peak-ring impact craters elsewhere on Mercury (Baker et al., 2011).

After their formation, peak-rings are subject to erosion, which can render them incomplete. Impact craters on Mercury often contain landforms known as "hollows" that are interpreted to have formed by the loss of a volatile component of the exhumed material due to sublimation (Blewett et al., 2011). There are many examples of impact features on Mercury, similar in age to Heaney, such as Raditladi and Lermontov, that show extensive hollowing (Blewett et al., 2013). However, it seems unlikely for this process to erode peak-rings entirely since hollows appear to have maximum depths of only several tens of meters (Blewett et al., 2011), compared with peak elements, which are generally several hundreds of meters high (Baker & Head, 2013). Furthermore, neither Heaney nor Bello shows evidence of pervasive hollowing in their crater walls (Thomas et al., 2014a), as one might expect if hollowing were responsible for eroding their peak-rings.

The most widespread erosive process on Mercury is impact cratering. In Heaney, there are no impact craters that postdate the smooth plains along the circle where a peak-ring would be expected to be found. Furthermore, it seems very unlikely that cratering predating the plains could have removed all but one peak of the ring. There are no "ghost craters" (Strom et al., 1975) in the smooth infill suggestive of impact overprinting of an originally complete peak-ring before smooth plains emplacement. Therefore, we believe that erosion of an originally complete peak-ring by hollowing or impact cratering is an improbable explanation for the prominence of CV1.

There are other impact crater morphologies, such as protobasin and complex crater, which Heaney could have originally exhibited with implications for the impact interpretation of the feature. The rings of peaks in protobasins on Mercury are lower in height than those of peak-ring basins and are often very incomplete with no evidence that the missing peak elements were removed after formation (Baker & Head, 2013) and so could be more easily buried by volcanism. If CV1 is a remnant peak-ring element of an original, incomplete protobasin then, as previously stated, it is at a somewhat greater radial distance from the center of Heaney than would be expected. Furthermore, the absence of any surface expression of an accompanying central peak requires the smooth plains to be very thick in the center of Heaney and much thinner at the edge. The central peaks and peak-rings in protobasins of Heaney's diameter are predicted to be ~1 km high (Baker & Head, 2013). This would require the smooth plains to be $>$1 km thick in the center of Heaney, to bury a central peak, but to be much thinner at the edges, to allow CV1 to remain unburied. This is not inconceivable, given our estimate of the maximum fill thickness (2 km), but it still requires very specific floor topography and a largely incomplete peak-ring. Finally, as Sūr Dās demonstrates (Figure 3d), it is possible that Heaney did not in fact form with a peak-ring at all, which would require a non-impact-related origin for CV1.

The red color associated with CV1 could be due to material exhumed from depth as part of a peak-ring. The reddish parts of the crater rim suggest that this is possible. However, if the other small knobs within Heaney are interpreted as remnant peak-ring elements, then the fact that they do not appear to have the same color anomaly would require the peak-ring to be compositionally diverse on short length scales. Furthermore, the

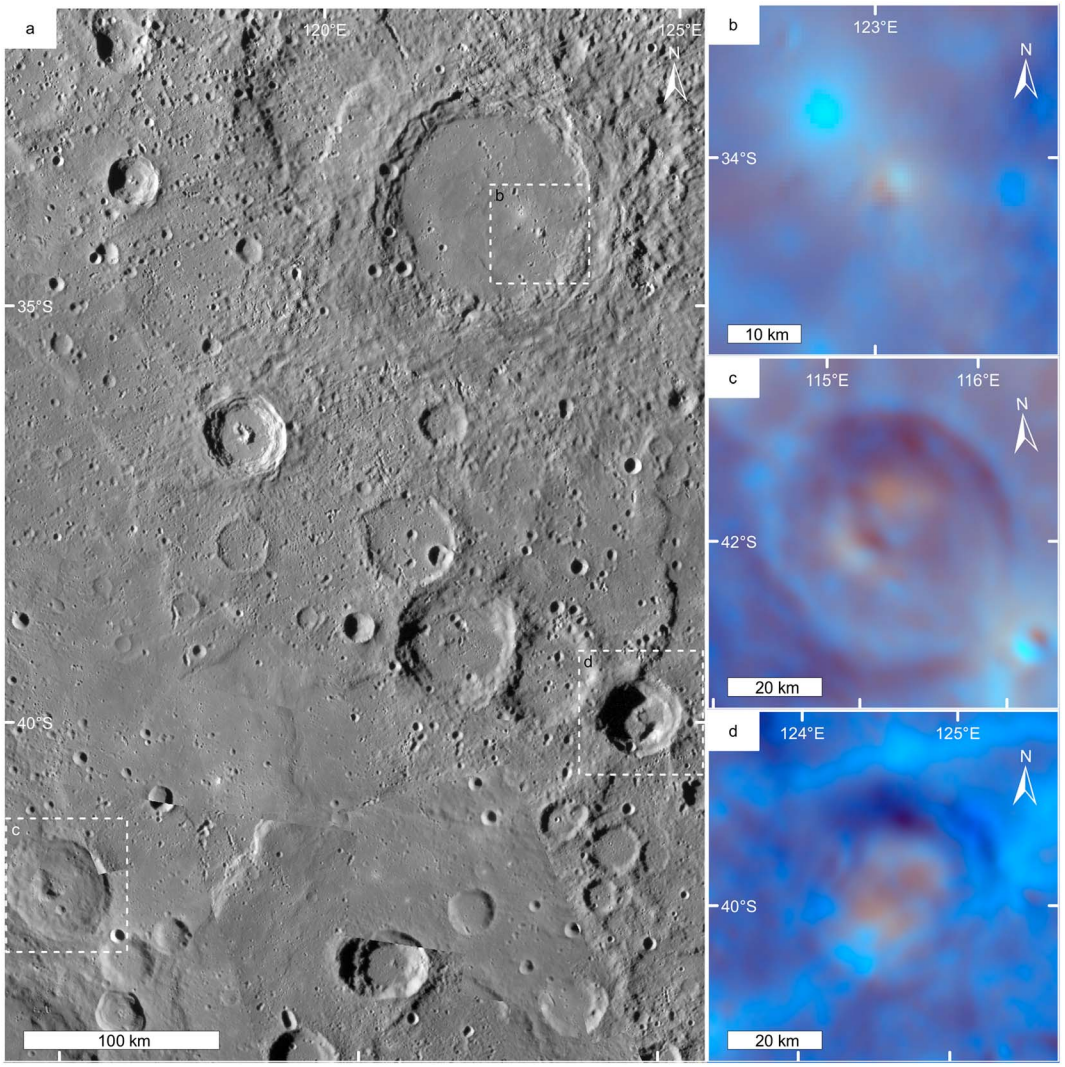

Figure 4. The locations of red color anomalies near Heaney. Depressions interpreted as pyroclastic vents are associated with the spectrally red anomalies of (c) and (d). (a) Context view showing the locations of the color anomalies in (b)–(d) (dashed white boxes). (b) Enhanced color view of the color anomalies in Heaney. (c) Red anomaly, interpreted as pyroclastic by Thomas et al. (2014b), within an unnamed crater (at 115.2°E, 42.0°S). (d) A similar color anomaly, interpreted as pyroclastic by Thomas et al. (2014b) within an unnamed crater (at 124.6°E, 39.9°S).

color contact between the low-reflectance blue plains crater infill and the embayed reddish crater rim is sharp, whereas the red color anomaly associated with CV1 is more diffuse. However, we acknowledge that these knobs occupy only a small number of pixels in available WAC images, meaning their spectral properties may not be sufficiently well characterized by MESSENGER.

3.1.3. Volcanic Interpretation

If CV1 is not a remnant peak-ring element, then it is plausible that it is a volcanic edifice of some kind. As mentioned previously, the thickness of the smooth infill is suggestive of postimpact volcanic activity occurring within Heaney. The red color anomaly is similar to those of identified pyroclastic deposits in impact craters elsewhere on Mercury (Figure 4; Thomas et al., 2014a). A dyke underneath CV1 may have supplied the smooth volcanic plains that cover the crater floor. A volcanic origin for CV1 avoids the problems outlined above for the impact interpretation. Under this volcanic scenario, any original peak-ring within Heaney that may have formed was completely buried by postimpact volcanism, which erupted directly from the crater floor, and CV1 was constructed afterward. The red color anomaly may be due to pyroclastics that were deposited by an explosive eruption (Thomas et al., 2015) that could have contributed to the excavation of the summit crater. If explosive eruptions did occur, this likely represented the final phase of volcanism in

Heaney. The northern flank depression is either part of a coincidental secondary impact crater chain or possibly a primary volcanic structure (see section 4.1). MESSENGER data are insufficient to rule out either of these hypotheses, although we have found no immediately obvious primary impact craters that could be ultimately responsible for the northern flank depression.

Elsewhere on Mercury, there is a close association between LRM, which is thought to bear surface-darkening carbon in the form of graphite (Peplowski et al., 2016), and sites of explosive volcanism (Thomas et al., 2015). The LRM evident in the southern rim and ejecta blanket of Heaney suggests that LRM is present beneath the crater (e.g., Ernst et al., 2015). Carbon is suggested to be an important volatile for driving pyroclastic volcanism on Mercury (Weider et al., 2016). The relatively red color of the pyroclastics is thought to be due in part to the removal of dark, spectrally blue carbon from the magma that leaves the remaining deposit red compared to the effusive plains around it (Weider et al., 2016). Concentration of volatiles, such as carbon, in the magma could result either from evolution in a shallow crustal magma chamber or by assimilation of volatiles from the surrounding crust and lead to an explosive eruption (Weider et al., 2016).

However, MESSENGER data are insufficient to establish an unequivocal volcanic origin for CV1. For instance, it is unclear at the available resolution whether CV1 superposes or is embayed by the smooth plains within Heaney. The impact uplift interpretation would be ruled out if CV1 superposes the plains, but if the smooth plains postdate it, then a volcanic origin is not assured. Furthermore, additional volcanic features (e.g., individual lava flows) cannot be seen around CV1. This could be merely due to the lack of resolution, however. For example, identifications of lava flow fronts elsewhere on Mercury based on morphological observations have proven to be equivocal (Byrne et al., 2013; Head et al., 2011).

The small, red color anomaly coincident with CV1 is poorly characterized in the available MESSENGER imagery. Heaney was imaged in WAC data only at high incidence angles (>45°), which are not ideal for assessing spectral properties, and at low spatial resolution (>600 m/pixel). Under these conditions, nearby Sun-facing slopes, such as parts of the crater wall of Heaney, also appear reddish. We therefore consider the presence of a small pyroclastic deposit at CV1, supporting its volcanic origin, to be equivocal as it is plausibly the result of misleading photometric effects. Nevertheless, the smooth infill, interpreted to be the product of postimpact volcanism, makes observations of volcanic color signatures in the region unsurprising. Moreover, an unequivocal color anomaly or identified pyroclastic deposit is not prerequisite for CV1 to have a volcanic origin.

3.2. Candidate Volcano #2

3.2.1. Observations

Candidate volcano #2 ("CV2") is located in the northwest of the Caloris basin rim, at 144°51′24″E, 44°30′49″N, and morphologically resembles CV1 (Figure 5). MLA data show that it has a convex-up shape and is 12.1 km in diameter, with an elevation above its surroundings of ~700 m. Treating it as a cone, CV2 has an average flank slope of 7°, in close agreement with the point-to-point slope method, which returns a median slope of 8°. Again, there is a summit depression, the internal shadow of which indicates that it is shallower than similarly sized impact craters nearby, as is the case for CV1. The ratio of the summit depression diameter to the basal diameter of CV2 (~0.21) is also similar to that of CV1. Conversely, CV2 has no associated color anomaly (see Figure S2 in the supporting information).

3.2.2. Interpretation

Other than having a summit depression, CV2 resembles the numerous knobs associated with the Caloris basin. These are most commonly interpreted as Caloris ejecta blocks, some of which have been embayed by smooth plains (Denevi et al., 2013; Fassett et al., 2009; McCauley et al., 1981), although it has also been suggested that these features are possibly "small volcanic constructs perhaps directly connected to the emplacement of the circum-Caloris plains" (Fassett et al., 2009). We consider the interpretation of CV2 as a volcanic edifice to be a plausible alternative to it being an ejecta block because of its morphological resemblance to CV1. The convex-up "shield" shape is consistent with a volcanic origin, whereas Caloris rim elements (Caloris Montes) are typically blocky and straight-sided (Fassett et al., 2009; McCauley et al., 1981; Rothery et al., 2017). The Caloris knobs described to the east of Caloris are smaller (i.e., have lower heights and typically smaller diameters) than CV2 (Ackiss et al., 2015). Though a statistically significant comparison of CV2 with Caloris knobs is beyond the scope of this study, knobs west of Caloris (closer to CV2) have comparable diameters but appear to be characterized by steeper flank slopes (Figure 6). CV2 is located just 15 km beyond the edge of Caloris Planitia, which was emplaced by smooth plains

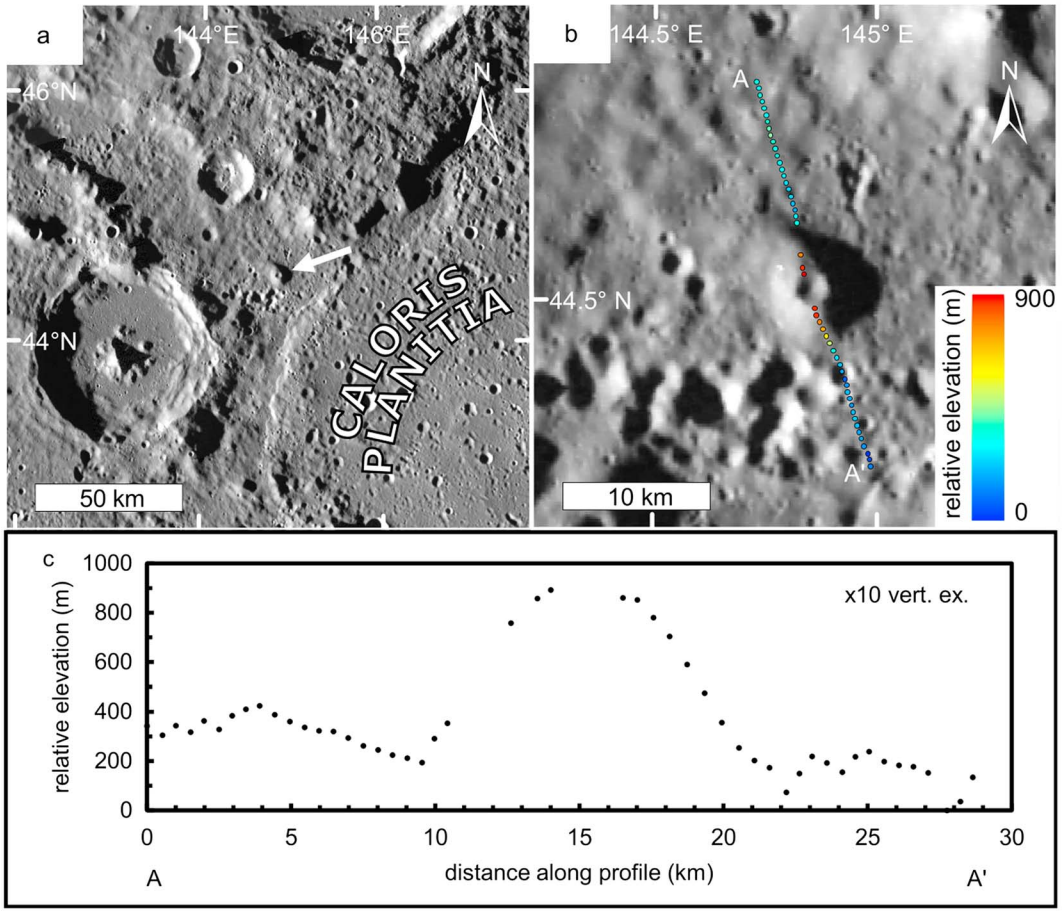

Figure 5. Photogeological and topographical observations of CV2. (a) The location of CV2 (white arrow) 15 km outside Caloris Planitia. (b) A larger-scale view of CV2 with dots marking locations of MLA data. The colors indicate the relative elevation. *A* and *A′* mark the ends of the topographic profile shown in (c). (c) MLA topographic profile of CV2.

volcanism (Denevi et al., 2009). The proximity of CV2 to this volcanic province means a volcanic origin for it must be considered. For example, vents attributed to explosive volcanism are concentrated within about 220 km of the Caloris rim (Murchie et al., 2008; Rothery et al., 2014) and other impact features elsewhere on Mercury (Thomas et al., 2014c).

4. Discussion

4.1. Comparison With Volcanic Edifices on Other Bodies

If these landforms are volcanic in origin, then they should compare favorably with other edifices throughout the solar system that are interpreted as volcanic. Given their sizes, we compare CV1 and CV2 to small volcanic landforms on Earth and the Moon.

There is no evidence that Mercury's lithosphere ever consisted of multiple tectonic plates (Solomon, 1978), so other single plate bodies and intraplate settings on Earth provide the most plausible analogues for CV1 and CV2. The most comparable Earth analogues in terms of size are small (<15 km in diameter), monogenetic shields, or cones, such as Mauna Ulu on the Island of Hawai'i (Swanson, 1973). Even interplate settings, such as Iceland, host monogenetic volcanoes that have formed in a similar manner to Hawai'ian examples (Thordarson & Larsen, 2007). Skjaldbreiður has an axisymmetric shape in plan view, as do CV1 and CV2, and a similar aspect ratio. The main difference between the Mercury landforms and Skjaldbreiður is the relative sizes of the summit craters: Skjaldbreiður has a crater-base diameter ratio of 3.75×10^{-3}, 2 orders of magnitude less than the corresponding ratios of the Mercury landforms. As stated previously, there is some color

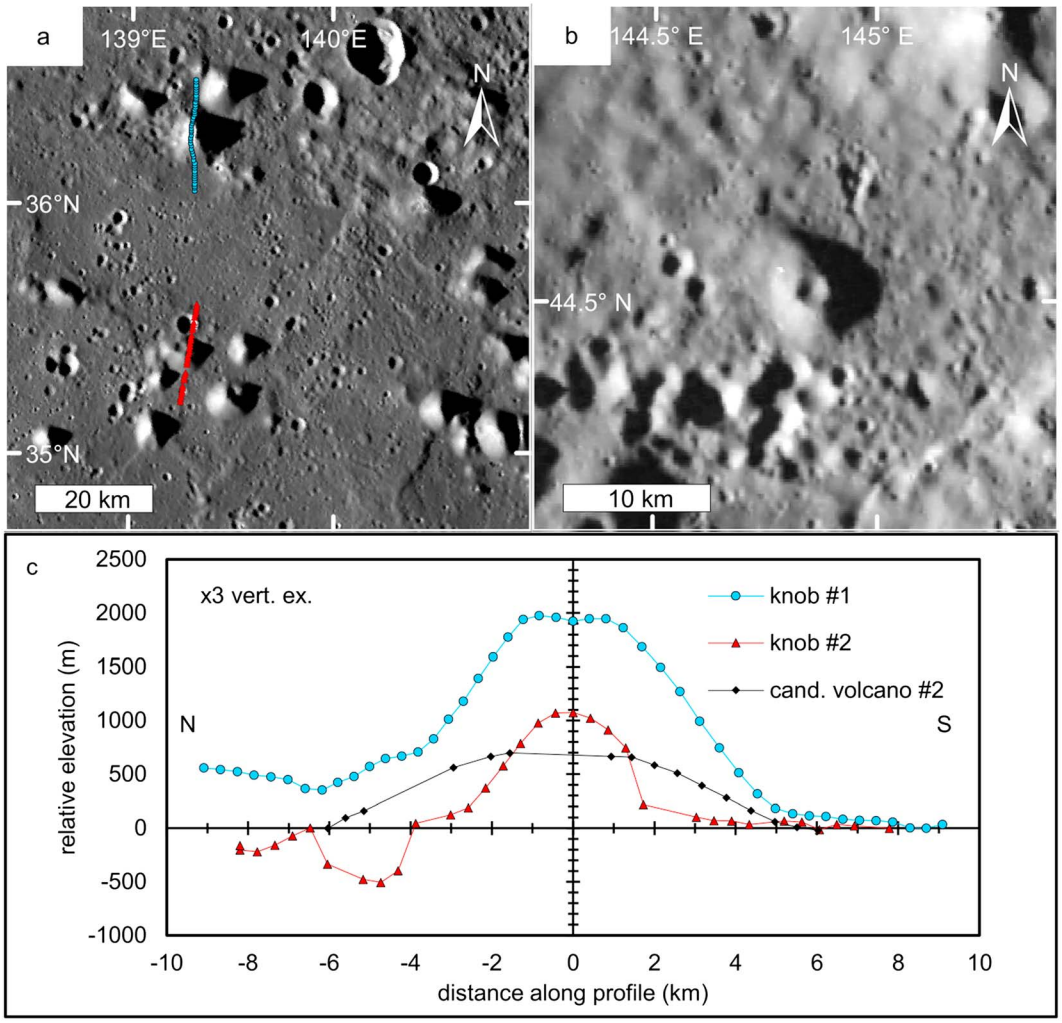

Figure 6. A morphological comparison of CV2 with knobs in the circum-Caloris plains. (a) An example of typical circum-Caloris knobs (with the image centered at 139.7°E, 35.7°N). The colored dots indicate MLA data points used to construct the profiles shown in (c). Fortuitously placed MLA tracks cross close to the peaks of these knobs. Inspection of the numerous other knobs in this view shows that those crossed by MLA tracks are likely to be representative of the population as a whole. (b) CV2 for comparison with circum-Caloris knobs. (c) MLA topographic profiles of two knobs shown in (a) as well as candidate volcano #2. All profiles are aligned N-S and shown with the same scale and vertical exaggeration. The circum-Caloris knobs have steeper slopes than does CV2.

evidence for explosive excavation of the summit crater at CV1 that is not evidenced to have occurred at Skjaldbreiður (Thordarson & Larsen, 2007). In any case, eruptions on Mercury are expected to have featured more vigorous fire-fountaining than those on Earth due to the rapid expansion of even a small volatile content within the magma under vacuum (Wilson & Head, 1981). This would also allow a wider summit crater to open than might happen on Earth (Kerber et al., 2009).

As airless bodies, comparisons of the products of volcanism on the Moon and Mercury are also potentially informative. Lunar mare domes (Figures 7c, 7d, and 8) provide an instructive comparison for the Mercury candidates. These landforms are low domes and are interpreted as small (<20 km-diameter) shield volcanoes (Head & Gifford, 1980). They are generally located toward the edges of the lunar maria or close to the edges of mare-hosting impact basins (McGovern & Litherland, 2011). The lunar maria frequently feature sinuous rilles, landforms that suggest that these plains were emplaced by high-effusion-rate lavas, with the mare domes thought to have formed toward the end of maria emplacement as effusion rates waned and lava flow lengths decreased (Wöhler et al., 2006).

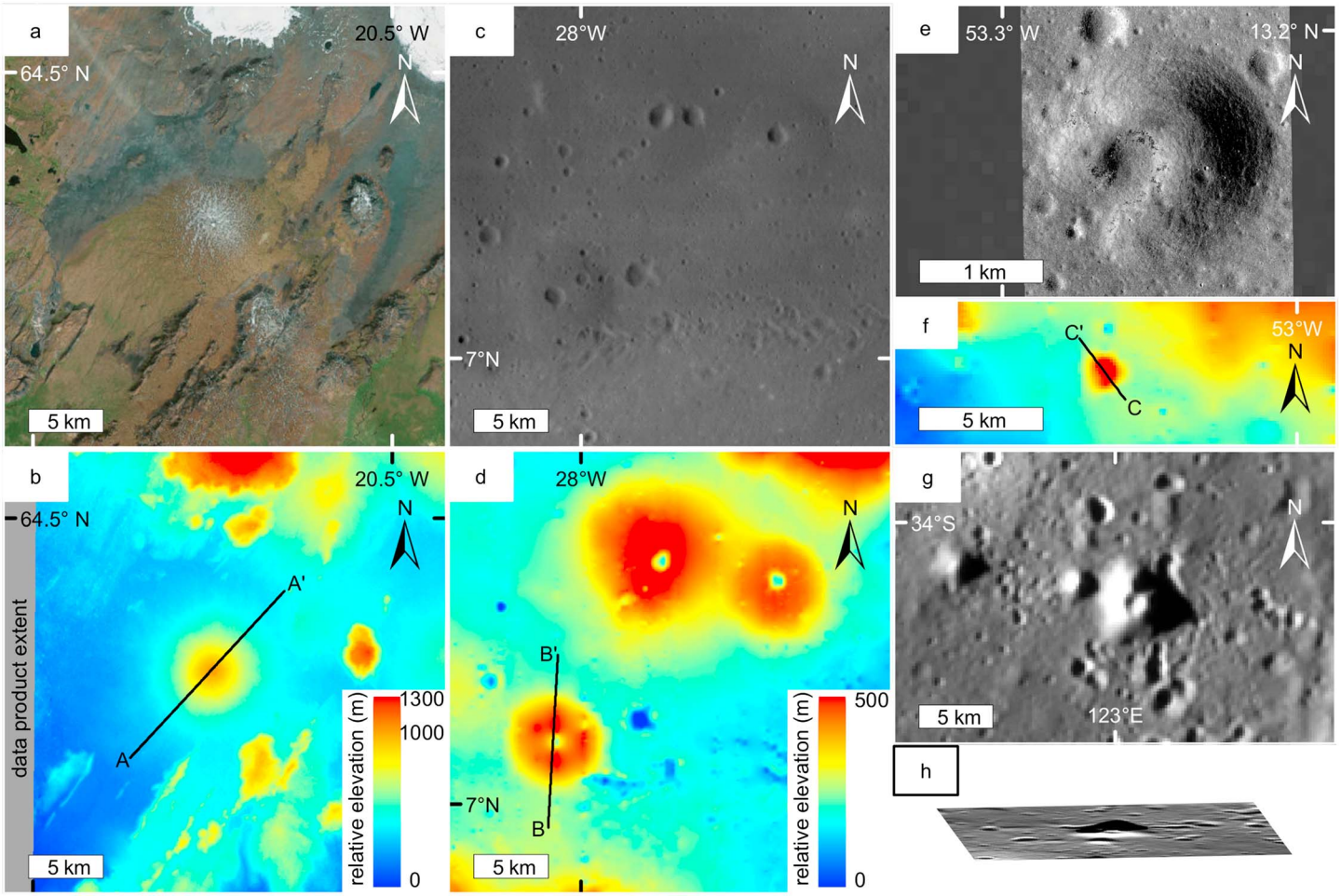

Figure 7. A comparison of select, small volcanic forms on several terrestrial bodies. (a) Skjaldbreiður, located in Iceland. (b) The topography of the Skjaldbreiður volcano (ASTER Global Digital Elevation Map v0002). The line marked *A-A′* indicates the cross section of Skjaldbreiður in Figure 8. (c) Lunar mare domes in Oceanus Procellarum. (d) Lunar mare dome topography (100-m/pixel LOLA data). The line marked *B-B′* indicates the cross section of lunar mare dome Hortensius 5 in Figure 8. (e) A putative cinder cone in the Marius Hills region on the Moon. Note its smaller size compared to the other volcanoes shown (LROC NAC frame M166195459RE). (f) Marius Hills cinder cone topography (100-m/pizel LOLA data). The line marked *C-C′* indicates the cross section of the cinder cone in Figure 8. (g) CV1 in Heaney crater, Mercury. (h) Warped image of CV1 used to determine approximate topographic profile (Figure 8) from its shadow according to the method of Basilevsky (2002). The specific data products used construct this figure are listed in Table S1.

As with the Mercury candidates, mare domes are generally circular and host summit craters that are shallower than impact craters of similar diameter (Head & Gifford, 1980). Lunar mare dome summit craters are also larger than terrestrial equivalents with one example, named Hortensius 5, within Mare Insularum, having a crater-base diameter ratio of ~0.33, much closer to those of the Mercury examples. The large sizes of the lunar mare dome summit depressions have been attributed to magma withdrawal from the conduit, causing the vent to collapse (Wöhler et al., 2006), and to the vigorous nature of eruptions into a vacuum (Head & Gifford, 1980). Both of these mechanisms can explain the large summit diameters of the candidate volcanoes on Mercury. If explosive activity did occur at CV1, as the color data suggest, then this may have contributed to the large size of the summit depression. At CV2, where there is no color evidence of an explosive volcanic deposit, magma withdrawal may have been the chief driver of summit depression enlargement.

Although mare domes have lower heights and shallower flank slopes than the prospective volcanoes on Mercury, this disparity can be explained by Mercury's higher surface gravity than the Moon. Stronger surface gravity leads to a less dispersed fire fountain where pyroclasts and spatter fall closer to the vent (Kerber et al., 2009), resulting in a steeper edifice. Furthermore, there are steeper putative volcanic constructs on the Moon in the Marius Hills region. Here there are steep domes (6–7° slopes) and cones (up to 17° slopes) with summit

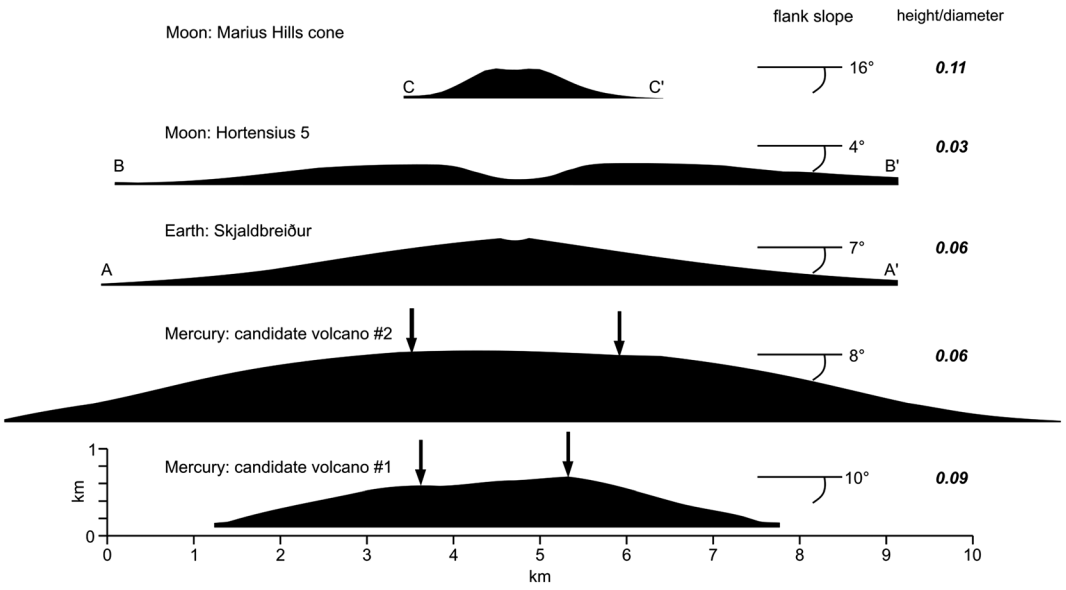

Figure 8. Comparisons of Mercury candidate volcanoes to small, volcanic landforms on Earth and the Moon. The black arrows indicate the extent of the summit depressions in each example where the topography of the depression cannot be resolved. The Mercury landforms have sizes comparable to an Icelandic shield volcano, and slopes intermediate between the examples of shield volcanoes and a lunar cinder cone shown here. No vertical exaggeration.

craters (Figures 7e, 7f, and 8) that are interpreted as constructs of varying degrees of lava and pyroclastics, superposed on lunar mare material (Lawrence et al., 2013; Weitz & Head, 1999). The domes are spectrally indistinct from the mare material, suggesting that eruption mechanics, rather than magma composition, are responsible for the switch from lava plains emplacement to shield construction. Cones in the Marius Hills often superpose the steep domes, indicating that they are the youngest volcanic forms in the region. These are interpreted as cinder cones that formed from terminal strombolian eruptions as the eruption rate waned further. Both the candidate volcanoes on Mercury we describe here have flank slopes intermediate between lunar shield volcanoes and lunar cinder cones. Most of the Marius Hills cones are C-shaped in plan view, possibly due to flows that overtopped the summit crater rim at its lowest point, eroding the cone walls (Lawrence et al., 2013). It is possible that this cone morphology is analogous to the northern flank depression of CV1. Other Marius Hills cones do not have such a gap, which makes them more similar to CV2 in appearance. The main difference between the Marius Hills cones and the candidate volcanoes on Mercury is size. The Marius Hills cones are typically 1–2 km across, whereas the CV1 and CV2 have diameters of ~6 and ~12 km, respectively. These diameters correspond more closely to those of lunar domes interpreted as shield volcanoes, although these features are not as steep as the Mercury landforms. This apparent discrepancy can be explained if the landforms on Mercury are composite volcanoes constructed by the accumulation of both lava and pyroclasts (Davidson & de Silva, 2000; Head, 1975).

4.2. Edifice Construction on Mercury

Whether or not CV1 and CV2 are volcanic edifices, it is apparent that Mercury's characteristic eruptive style during its early history overwhelmingly generated widespread volcanic plains, with edifice construction occurring either very rarely or not at all. Borealis Planitia and the Caloris smooth plains, believed to represent the most recent, large-scale effusive volcanic activity, have model ages of ~3.7 Ga (Denevi et al., 2013; Head et al., 2011; Ostrach et al., 2015). Shortly after this time, at about 3.5 Ga, large-scale effusive volcanism on Mercury appears to have ceased across the planet (Byrne et al., 2016). This cessation was likely in response to magma ascent pathways being closed by global contraction (Byrne et al., 2016; Solomon, 1978; Wilson & Head, 2008). As cooling and contraction of Mercury's interior continued after the end of widespread effusive volcanism, magma is predicted to have stalled at ever increasing depths beneath the planet's surface (Maccaferri, Bonafede, & Rivalta, 2011; Menand, Daniels, & Benghiat, 2010). However, impacts remove overburden, promote uplift, temporarily reset the preexisting stress regime, propagate fractures, and deposit heat, all of which could facilitate the generation and extraction of magma from the subsurface (Byrne

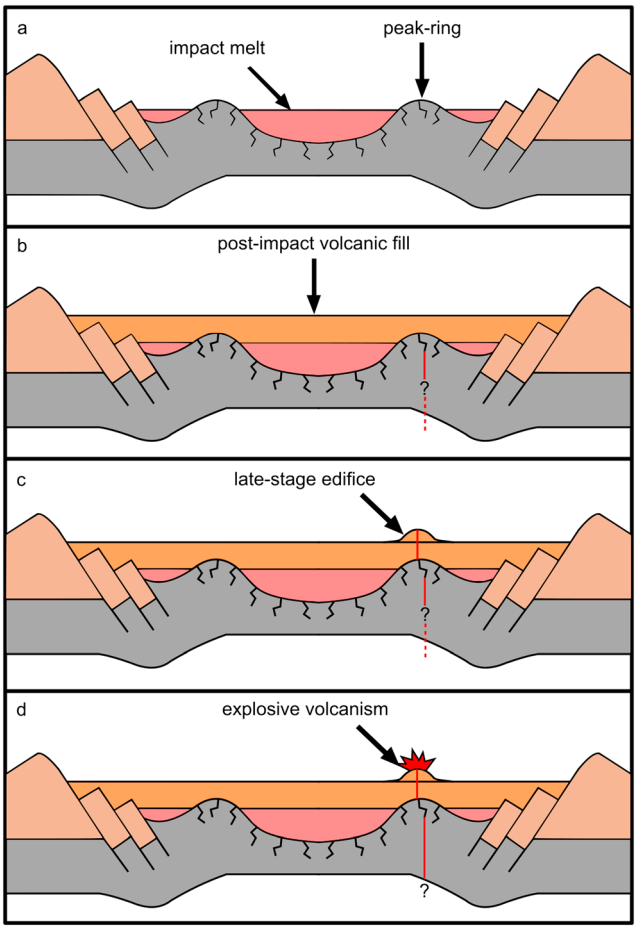

Figure 9. Conceptual model of formation of candidate volcano #1 (CV1). Heaney is shown as a peak-ring basin, but this model would also apply to a protobasin morphology. (a) Heaney formed as a crater with a peak-ring after the end of widespread effusive eruptions, but before magmagenesis in the subsurface was inhibited due to secular cooling of the planet's interior. The impact propagated fractures within, and temporarily reset the compressive regime in, the preexisting crust. (b) A small volume of mantle-derived magma was liberated from storage in the crust by exploiting fractures formed by the impact. (c) The global compressive regime began to affect the region toward the end of effusive volcanism in the crater, such that subsequent eruptions were concentrated above the peak-ring. CV1 was built as a result of late-stage, small-volume lava flows from a single source. (d) When the magma rise rate became critically low, it is possible that a switch to an explosive style occurred due to the concentration of volatiles in the magma, leaving a final pyroclastic deposit.

et al., 2016). Therefore, impact craters that formed a sufficiently short time after the end of widespread effusive volcanism on Mercury are arguably more likely than other locations to host late-stage volcanism.

We therefore propose a sequence of events that led to the formation of CV1 that is both consistent with our observations and explains the paucity of constructional edifices on the planet in general (Figure 9). The late Calorian/early Mansurian appearance of Heaney crater means it likely formed toward the end of, or after, widespread effusive volcanism on Mercury, but probably when crustal magma intrusion was still occurring (~3.5 Ga; Byrne et al., 2016). Postimpact volcanism has been recognized in impact features elsewhere on Mercury dating from this time period or later (Blair et al., 2013; Prockter et al., 2010). Crustal storage and intrusion permitted the melt to become more evolved (thus increasing the magma viscosity) and/or assimilate crustal volatiles (Thomas et al., 2015). Due to the effects of impacts listed above, the crater was filled by late-stage, postimpact effusive volcanism that buried any original peak-ring that might have formed. The erupted volumes of this postimpact volcanism were much lower than during the emplacement of the extensive smooth plains on Mercury because only magma stored locally beneath the impact site could be mobilized. This is similar to the small volumes of magma mobilized from shallow magma chambers theorized to form the domes and cones of the Marius Hills (Heather, Dunkin, & Wilson, 2003).

To begin with, eruptions may have occurred at multiple locations within the crater, but the peak-ring area could have been favored by the presence of deep, high-angle bounding normal faults (Kenkmann, Poelchau, & Wulf, 2014). Lunar mare domes, for example, are also associated with such structural features (Head & Gifford, 1980). Following the initial postimpact volcanism, the effusion rate slowed as Mercury's global horizontally compressive stress regime began to reassert itself. Evidence for this effect globally comes in the form of small, young lobate scarps elsewhere (Watters et al., 2016). Heaney's smooth infill could be accommodating strain due to Mercury's stress regime similarly, since the infill contains possible small-scale wrinkle ridges. Alternatively, these ridges may have formed due to natural subsidence of the smooth infill, evidenced to have occurred to some degree by Heaney's concave-up interior topography. Subsidence could drive shallow folding and thrust faulting, resulting in wrinkle ridge formation (Blair et al., 2013). In either case, we expect the stress regime within the crater to have become increasingly horizontally compressive following the impact. If the reassertion of such a stress field upon the interior of Heaney were geologically rapid, then any postimpact volcanism must have commenced relatively quickly after the impact. This is a plausible scenario, since no ghost craters are seen in the smooth infill of Heaney, suggesting that little geological time passed between crater formation and volcanic infilling. The increasingly horizontally compressive stress regime closed magma ascent pathways until eruptions were concentrated at a single vent at the location of CV1, which is plausibly situated above the buried peak-ring. The lower effusion rate, small erupted volume, and single source vent led to the construction of a prominent volcano toward the end of this sequence. Construction may have been enhanced by the erupted lavas having higher crystallinity, lower eruption temperatures, and more evolved compositions (Namur & Charlier, 2017) than typical plains-forming lavas on Mercury. Eventually, the effects of the impact that had mobilized the magma diminished and effusion ceased. The final eruption(s) occurred in the style of other explosive eruptions elsewhere on Mercury: The exsolution of volatiles concentrated in the magma by subsurface evolution and/or crustal assimilation caused the last melt to ascend rapidly from depth, leading to a final phase of explosive volcanic activity

before the extinction of the volcano (Thomas et al., 2015). This last phase of explosive volcanism must have been short-lived and was possibly a single event of sufficiently small scale to explain the correspondingly small size of the resultant pyroclastic deposit compared with other red spots on Mercury (Thomas et al., 2014c) and the preservation of the constructional edifice. No observations we have made of Heaney crater require that significant intervals of geological time separate the impact event, the burial of the crater floor by smooth plains, the construction of the edifice, or the final explosive eruptive phase. Therefore, based on studies of postimpact volcanism elsewhere on Mercury (Chapman et al., 2012; Ferrari et al., 2015; Prockter et al., 2010), we tentatively suggest that this whole sequence of events was completed in under 100 million years.

It may be that CV2 formed in a similar manner. In this case, toward the end of the emplacement of the Caloris plains, late-stage, low-volume eruptions ascended along a fracture associated with the rim of the Caloris basin. The known explosive vents within Caloris Planitia are within 220 km of the edge of the basin (Besse, Doressoundiram, & Benkhoff, 2015; Thomas et al., 2014c). Sites of young lunar volcanism are also concentrated toward the edges of the lunar maria (Head & Gifford, 1980). This is thought to be due to the magma ascent-enhancing stress state found at mare basin margins. Lithospheric loads, such as the lunar maria or Caloris Planitia, can cause extension in an annulus close to the edge of the load, assisting magma ascent (McGovern & Litherland, 2011). Furthermore, small-volume magmas may preferentially erupt close to the edge of Caloris Planitia, where the basin-filling lavas are thinnest, since their overburden stresses would pose the least obstacle to magma ascent there (Rothery et al., 2014).

5. Conclusions

To date, no constructional volcanic edifices have been unambiguously identified on Mercury. We have appraised two positive-relief landforms on the planet as candidate constructional volcanic edifices, although we cannot rule out nonvolcanic hypotheses for their origins with MESSENGER data. Nevertheless, the fact that few prospective constructional volcanic edifices have been reported on Mercury is important. Any small constructional volcanic edifices that do exist on Mercury likely represent only a fraction of those that ever formed, since edifices are subject to erosion, particularly due to destruction by subsequent impacts. However, numerous small volcanic constructs exist on the Moon (Head & Gifford, 1980), which has had a similar history of impact erosion to Mercury (Fassett & Minton, 2013), indicating that if small-scale edifice construction is widespread enough, evidence that it occurred can survive billions of years of geological time. On this basis, we argue that edifice construction on Mercury must have been highly spatiotemporally constrained throughout its geological history, assuming such construction occurred at all. We suggest that the scarcity of candidate volcanic edifices on Mercury is not a product of their removal by erosion but instead reflects the availability of small-volume, short flow length, high-viscosity eruptions. Eruptions of this kind appear to have been very unusual, since volcanism during Mercury's early history primarily formed widespread plains. Large-scale effusive volcanism came to a geologically abrupt end globally ~3.5 Ga, most likely in response to global contraction (Byrne et al., 2016). This contrasts with the more protracted decline of effusive volcanism on the Moon (Hiesinger et al., 2000), which could explain the dearth of volcanic edifices on Mercury. The first candidate edifice we have described here may have been able to form due to the small erupted volume of material capable of ascending into an impact crater postdating widespread effusive volcanism. This is similar to how monogenetic volcanoes on Earth and other terrestrial planets are thought to form from small volumes of lava. Assuming Heaney has the minimum diameter required to extract small-volume melts, we conservatively estimate that there are ~26 impact features on Mercury of sufficient size and youth to host constructional edifices (see Table S2 in the supporting information). Other than Heaney, none of these appears to host edifices with summit depressions similar to our candidates, but they may host less topographically pronounced domes that cannot be identified using MESSENGER data. Our second candidate edifice could be the result of final, small melt volumes erupting toward the end of the emplacement of the Caloris smooth plains, similar to the formation of lunar mare domes after most of the mare basalts were emplaced.

Our interpretations for these two candidate volcanic edifices lead us to conclude that (1) volcanic edifices could be found in other impact craters that formed shortly after the end of widespread effusive volcanism on Mercury, controlled by impact-related fractures in the subsurface; (2) edifices are unlikely to be found

toward the center of thick volcanic plateaus, as magma capable of forming edifices are better able to ascend to the surface through the reduced overburden and favorable stress fields at the edges of plateaus (McGovern & Litherland, 2011); and (3) edifices are not expected to be found in more ancient impact craters that formed when widespread plains emplacement was still occurring globally, as the erupted volumes and effusion rates are predicted to be too high. No edifices have, to date, been recognized in the smooth plains within the Beethoven basin, for example, or other pre-Calorian impact basins and craters (Fassett et al., 2012).

Although MESSENGER data are sufficient to search for features such as those we describe here the arrival of the BepiColombo spacecraft (Rothery et al., 2010) will enable a new search for prospective small volcanoes on the innermost planet. High-resolution (approaching 5 m/pixel), stereo (~50 m/pixel), and multispectral images (Benkhoff et al., 2010) will enable more detailed observations of the surface, facilitating the search for additional volcanoes on Mercury, such as low domes or cones without large summit craters, should they be present. BepiColombo will also be able to test the origin of the two landforms, volcanic or otherwise, we describe here.

Acknowledgments
The planetary data products used in this paper are publicly available from the Planetary Data System (PDS). MESSENGER data are credited to NASA/Johns Hopkins University Applied Physics Laboratory/Carnegie Institute of Washington. The lunar image and topographical data are credited to the LROC and LOLA teams, respectively. Earth imagery was supplied by DigitalGlobe and ESRI. ASTER Global Digital Elevation Map is a product of NASA and METI. J.W. was funded by the UK Science and Technology Facilities Council (STFC) under grant ST/N50421X/1 and is also grateful to the British Society for Geomorphology and the Remote Sensing and Photogrammetry Society for providing additional funding during the completion of this study. D.A.R. was supported by the UK Space Agency and STFC under grants ST/M002101/1, ST/L000776/1, and ST/N00399X/1. The authors are grateful to Paul Byrne and an anonymous reviewer for thoughtful and comprehensive reviews that greatly improved the quality of this manuscript. The authors also wish to thank Carolyn Ernst and Eric Christiansen for reviews of an earlier draft of this manuscript. The authors declare no conflicts of interest.

References

Ackiss, S. E., Buczkowski, D. L., Ernst, C. M., McBeck, J. A., & Seelos, K. D. (2015). Knob heights within circum-Caloris geologic units on Mercury: Interpretations of the geologic history of the region. *Earth and Planetary Science Letters*, *430*, 542–550. https://doi.org/10.1016/j.epsl.2015.08.003

Aschauer, J., & Kenkmann, T. (2017). Impact cratering on slopes. *Icarus*, *290*, 89–95. https://doi.org/10.1016/j.icarus.2017.02.021

Baker, D. M. H., & Head, J. W. (2013). New morphometric measurements of craters and basins on Mercury and the Moon from MESSENGER and LRO altimetry and image data: An observational framework for evaluating models of peak-ring basin formation. *Planetary and Space Science*, *86*, 91–116. https://doi.org/10.1016/j.pss.2013.07.003

Baker, D. M. H., Head, J. W., Schon, S. C., Ernst, C. M., Prockter, L. M., Murchie, S. L., et al. (2011). The transition from complex crater to peak-ring basin on Mercury: New observations from MESSENGER flyby data and constraints on basin formation models. *Planetary and Space Science*, *59*(15), 1932–1948. https://doi.org/10.1016/j.pss.2011.05.010

Banks, M. E., Xiao, Z., Braden, S. E., Barlow, N. G., Chapman, C. R., Fassett, C. I., & Marchi, S. (2017). Revised constraints on absolute age limits for Mercury's Kuiperian and Mansurian stratigraphic systems. *Journal of Geophysical Research: Planets*, *122*, 1010–1020. https://doi.org/10.1002/2016JE005254

Barnouin, O. S., Zuber, M. T., Smith, D. E., Neumann, G. A., Herrick, R. R., Chappelow, J. E., et al. (2012). The morphology of craters on Mercury: Results from MESSENGER flybys. *Icarus*, *219*(1), 414–427. https://doi.org/10.1016/j.icarus.2012.02.029

Basilevsky, A. T. (2002). Morphology of Callisto Knobs from photogeologic analysis of Galileo SSI images taken at Orbit C21. In 33rd Lunar and Planetary Science Conference (2002), Abstract 1014.

Becker, K. J., Robinson, M. S., Becker, T. L., Weller, L. A., Edmundson, K. L., Neumann, G. A., et al. (2016). First global digital elevation model of Mercury. In 47th Lunar and Planetary Science Conference (2016), Abstract 2959.

Benkhoff, J., van Casteren, J., Hayakawa, H., Fujimoto, M., Laakso, H., Novara, M., et al. (2010). BepiColombo—Comprehensive exploration of Mercury: Mission overview and science goals. *Planetary and Space Science*, *58*(1-2), 2–20. https://doi.org/10.1016/j.pss.2009.09.020

Besse, S., Doressoundiram, A., & Benkhoff, J. (2015). Spectroscopic properties of explosive volcanism within the Caloris basin with MESSENGER observations. *Journal of Geophysical Research: Planets*, *120*, 2102–2117. https://doi.org/10.1002/2015JE004819

Blair, D. M., Freed, A. M., Byrne, P. K., Klimczak, C., Prockter, L. M., Ernst, C. M., et al. (2013). The origin of graben and ridges in Rachmaninoff, Raditladi, and Mozart basins, Mercury. *Journal of Geophysical Research: Planets*, *118*, 47–58. https://doi.org/10.1029/2012JE004198

Blewett, D. T., Chabot, N. L., Denevi, B. W., Ernst, C. M., Head, J. W., Izenberg, N. R., et al. (2011). Hollows on Mercury: MESSENGER evidence for geologically recent volatile-related activity. *Science*, *333*(6051), 1856–1859. https://doi.org/10.1126/science.1211681

Blewett, D. T., Vaughan, W. M., Xiao, Z., Chabot, N. L., Denevi, B. W., Ernst, C. M., et al. (2013). Mercury's hollows: Constraints on formation and composition from analysis of geological setting and spectral reflectance. *Journal of Geophysical Research: Planets*, *118*, 1013–1032. https://doi.org/10.1029/2012JE004174

Browne, P. R. L., & Lawless, J. V. (2001). Characteristics of hydrothermal eruptions, with examples from New Zealand and elsewhere. *Earth Science Reviews*, *52*(4), 299–331. https://doi.org/10.1016/S0012-8252(00)00030-1

Bryan, S. E., & Ernst, R. E. (2008). Revised definition of Large Igneous Provinces (LIPs). *Earth-Science Reviews*, *86*(1–4), 175–202. https://doi.org/10.1016/j.earscirev.2007.08.008

Byrne, P. K., Klimczak, C., Williams, D. A., Hurwitz, D. M., Solomon, S. C., Head, J. W., et al. (2013). An assemblage of lava flow features on Mercury. *Journal of Geophysical Research: Planets*, *118*, 1303–1322. https://doi.org/10.1002/jgre.20052

Byrne, P. K., Ostrach, L. R., Fassett, C. I., Chapman, C. R., Denevi, B. W., Evans, A. J., et al. (2016). Widespread effusive volcanism on Mercury likely ended by about 3.5 Ga. *Geophysical Research Letters*, *43*, 7408–7416. https://doi.org/10.1002/2016GL069412

Cavanaugh, J. F., Smith, J. C., Sun, X., Bartels, A. E., Ramos-Izquierdo, L., Krebs, D. J., et al. (2007). The Mercury Laser Altimeter Instrument for the MESSENGER mission. *Space Science Reviews*, *131*(1–4), 451–479. https://doi.org/10.1007/s11214-007-9273-4

Chabot, N. L., Denevi, B. W., Murchie, S. L., Hash, C. D., Ernst, C. M., Blewett, D. T., et al. (2016). Mapping Mercury: Global Imaging strategy and products from the MESSENGER mission. In 47th Lunar and Planetary Science Conference, Abstract 1256.

Chapman, C. R., Merline, W. J., Marchi, S., Prockter, L. M., Fassett, C. I., Head, J. W., et al. (2012). The Young Inner Plains of Mercury's Rachmaninoff basin reconsidered. In 43rd Lunar and Planetary Science Conference, Abstract 1607.

Chin, G., Brylow, S., Foote, M., Garvin, J., Kasper, J., Keller, J., et al. (2007). Lunar reconnaissance orbiter overview: The instrument suite and mission. *Space Science Reviews*, *129*(4), 391–419. https://doi.org/10.1007/s11214-007-9153-y

Cintala, M. J., & Grieve, R. A. F. (1998). Scaling impact melting and crater dimensions: Implications for the lunar cratering record. *Meteoritics & Planetary Science*, *33*(4), 889–912. https://doi.org/10.1111/j.1945-5100.1998.tb01695.x

Davidson, J., & de Silva, S. (2000). Composite volcanoes. In *Encyclopedia of volcanoes* (pp. 663–681). San Diego, CA: Academic Press.
Denevi, B. W., Ernst, C. M., Meyer, H. M., Robinson, M. S., Murchie, S. L., Whitten, J. L., et al. (2013). The distribution and origin of smooth plains on Mercury. *Journal of Geophysical Research: Planets*, *118*, 891–907. https://doi.org/10.1002/jgre.20075
Denevi, B. W., Robinson, M. S., Solomon, S. C., Murchie, S. L., Blewett, D. T., Domingue, D. L., et al. (2009). The evolution of Mercury's crust: A global perspective from MESSENGER. *Science*, *324*(5927), 613–618. https://doi.org/10.1126/science.1172226
Denevi, B. W., Seelos, F. P., Ernst, C. M., Keller, M. R., Chabot, N. L., Murchie, S. L., et al. (2016). Final calibration and multispectral map products from the Mercury Dual Imaging System wide-angle camera on MESSENGER. In 47th Lunar and Planetary Science Conference, Abstract 1264.
Ernst, C. M., Denevi, B. W., Barnouin, O. S., Klimczak, C., Chabot, N. L., Head, J. W., et al. (2015). Stratigraphy of the Caloris basin, Mercury: Implications for volcanic history and basin impact melt. *Icarus*, *250*, 413–429. https://doi.org/10.1016/j.icarus.2014.11.003
Fassett, C. I., Crowley, M. C., Leight, C., Dyar, M. D., Minton, D. A., Hirabayashi, M., et al. (2017). Evidence for rapid topographic evolution and crater degradation on Mercury from simple crater morphometry. *Geophysical Research Letters*, *44*, 5326–5335. https://doi.org/10.1002/2017GL073769
Fassett, C. I., Head, J. W., Baker, D. M. H., Zuber, M. T., Smith, D. E., Neumann, G. A., et al. (2012). Large impact basins on Mercury: Global distribution, characteristics, and modification history from MESSENGER orbital data. *Journal of Geophysical Research*, *117*, E00L08. https://doi.org/10.1029/2012JE004154
Fassett, C. I., Head, J. W., Blewett, D. T., Chapman, C. R., Dickson, J. L., Murchie, S. L., et al. (2009). Caloris impact basin: Exterior geomorphology, stratigraphy, morphometry, radial sculpture, and smooth plains deposits. *Earth and Planetary Science Letters*, *285*(3–4), 297–308. https://doi.org/10.1016/j.epsl.2009.05.022
Fassett, C. I., & Minton, D. A. (2013). Impact bombardment of the terrestrial planets and the early history of the Solar System. *Nature Geoscience*, *6*(7), 520–524. https://doi.org/10.1038/ngeo1841
Ferrari, S., Massironi, M., Marchi, S., Byrne, P. K., Klimczak, C., Martellato, E., & Cremonese, G. (2015). Age relationships of the Rembrandt basin and Enterprise Rupes, Mercury. *Geological Society, London, Special Publications*, *401*(1), 159–172. https://doi.org/10.1144/SP401.20
Goudge, T. A., Head, J. W., Kerber, L., Blewett, D. T., Denevi, B. W., Domingue, D. L., et al. (2014). Global inventory and characterisation of pyroclastic deposits on Mercury: New insights into pyroclastic activity from MESSENGER orbital data. *Journal of Geophysical Research: Planets*, *119*, 635–658. https://doi.org/10.1002/2013JE004480
Greeley, R. (1982). The Snake River Plain, Idaho—Representative of a new category of volcanism. *Journal of Geophysical Research*, *87*(B4), 2705–2712. https://doi.org/10.1029/JB087iB04p02705
Grieve, R. A. F., & Cintala, M. J. (1992). An analysis of differential impact melt-crater scaling and implications for the terrestrial impact record. *Meteoritics*, *27*(5), 526–538. https://doi.org/10.1111/j.1945-5100.1992.tb01074.x
Hauber, E., Bleacher, J., Gwinner, K., Williams, D. A., & Greeley, R. (2009). The topography and morphology of low shields and associated landforms of plains volcanism in the Tharsis region of Mars. *Journal of Volcanology and Geothermal Research*, *185*(1–2), 69–95. https://doi.org/10.1016/j.jvolgeores.2009.04.015
Hawkins, S. E., Boldt, J. D., Darlington, E. H., Espiritu, R., Gold, R. E., Gotwols, B., et al. (2007). The Mercury Dual Imaging System on the MESSENGER spacecraft. *Space Science Reviews*, *131*(1–4), 247–338. https://doi.org/10.1007/s11214-007-9266-3
Head, J. W. (1975). Morphology of pyroclastic lunar volcanic deposits: Implications for eruption conditions and localized sources of volatiles. In 6th Lunar and Planetary Science Conference, Abstract 349.
Head, J. W., Chapman, C. R., Strom, R. G., Fassett, C. I., Denevi, B. W., Blewett, D. T., et al. (2011). Flood volcanism in the northern high latitudes of Mercury revealed by MESSENGER. *Science*, *333*(6051), 1853–1856. https://doi.org/10.1126/science.1211997
Head, J. W., & Gifford, A. (1980). Lunar mare domes: Classification and modes of origin. *The Moon and Planets*, *22*(2), 235–258. https://doi.org/10.1007/BF00898434
Head, J. W., Murchie, S. L., Prockter, L. M., Robinson, M. S., Solomon, S. C., Strom, R. G., et al. (2008). Volcanism on Mercury: Evidence from the first MESSENGER flyby. *Science*, *321*(5885), 69–72. https://doi.org/10.1126/science.1159256
Heather, D. J., Dunkin, S. K., & Wilson, L. (2003). Volcanism on the Marius Hills plateau: Observational analyses using Clementine multispectral data. *Journal of Geophysical Research*, *108*(E3), 5017. https://doi.org/10.1029/2002JE001938
Hiesinger, H., Jaumann, R., Neukum, G., & Head, J. W. (2000). Ages of mare basalts on the lunar nearside. *Journal of Geophysical Research*, *105*(E12), 29,239–29,275. https://doi.org/10.1029/2000JE001244
Jozwiak, L. M., Head, J. W., & Wilson, L. (2018). Explosive volcanism on Mercury: Analysis of vent and deposit morphology and modes of eruption. *Icarus*, *302*, 191–212. https://doi.org/10.1016/j.icarus.2017.11.011
Kenkmann, T., Poelchau, M. H., & Wulf, G. (2014). Structural geology of impact craters. *Journal of Structural Geology*, *62*, 156–182. https://doi.org/10.1016/j.jsg.2014.01.015
Kerber, L., Head, J. W., Blewett, D. T., Solomon, S. C., Wilson, L., Murchie, S. L., et al. (2011). The global distribution of pyroclastic deposits on Mercury: The view from MESSENGER flybys 1-3. *Planetary and Space Science*, *59*(15), 1895–1909. https://doi.org/10.1016/j.pss.2011.03.020
Kerber, L., Head, J. W., Solomon, S. C., Murchie, S. L., Blewett, D. T., & Wilson, L. (2009). Explosive volcanic eruptions on Mercury: Eruption conditions, magma volatile content, and implications for interior volatile abundances. *Earth and Planetary Science Letters*, *285*(3–4), 263–271. https://doi.org/10.1016/j.epsl.2009.04.037
Kinczyk, M. J., Prockter, L. M., Chapman, C. R., & Susorney, H. C. M. (2016). A morphological evaluation of crater degradation on Mercury: Revisiting crater classification with MESSENGER data. In 47th Lunar and Planetary Science Conference, Abstract 1573.
Kneissl, T., Van Gasselt, S., & Neukum, G. (2011). Map-projection-independent crater size-frequency determination in GIS environments—New software tool for ArcGIS. *Planetary and Space Science*, *59*(11–12), 1243–1254. https://doi.org/10.1016/j.pss.2010.03.015
Kreslavsky, M. A., & Head, J. W. (1999). Kilometer-scale slopes on Mars and their correlation with geologic units: Initial results from Mars Orbiter Laser Altimeter (MOLA) data. *Journal of Geophysical Research: Planets*, *104*(E9), 21,911–21,924. https://doi.org/10.1029/1999JE001051
Lawrence, S. J., Stopar, J. D., Hawke, B. R., Greenhagen, B. T., Cahill, J. T. S., Bandfield, J. L., et al. (2013). LRO observations of morphology and surface roughness of volcanic cones and lobate lava flows in the Marius Hills. *Journal of Geophysical Research: Planets*, *118*, 615–634. https://doi.org/10.1002/jgre.20060
Le Feuvre, M., & Wieczorek, M. A. (2011). Nonuniform cratering of the Moon and a revised crater chronology of the inner Solar System. *Icarus*, *214*(1), 1–20. https://doi.org/10.1016/j.icarus.2011.03.010
Maccaferri, F., Bonafede, M., & Rivalta, E. (2011). A quantitative study of the mechanisms governing dike propagation, dike arrest and sill formation. *Journal of Volcanology and Geothermal Research*, *208*(1–2), 39–50. https://doi.org/10.1016/j.jvolgeores.2011.09.001
Marchi, S., Mottola, S., Cremonese, G., Massironi, M., & Martellato, E. (2009). A new chronology for the Moon and Mercury. *The Astronomical Journal*, *137*(6), 4936–4948. https://doi.org/10.1088/0004-6256/137/6/4936

McCauley, J. F., Guest, J. E., Schaber, G. G., Trask, N. J., & Greeley, R. (1981). Stratigraphy of the Caloris basin, Mercury. *Icarus*, *47*(2), 184–202. https://doi.org/10.1016/0019-1035(81)90166-4

McGovern, P. J., & Litherland, M. M. (2011). Lithospheric stress and basaltic magma ascent on the Moon, with implications for large volcanic provinces and edifices. 42nd Lunar and Planetary Science Conference, Abstract 2587. https://doi.org/10.1038/NGEO897

Menand, T., Daniels, K. A., & Benghiat, P. (2010). Dyke propagation and sill formation in a compressive tectonic environment. *Journal of Geophysical Research*, *115*, B08201. https://doi.org/10.1029/2009JB006791

Murchie, S. L., Watters, T. R., Robinson, M. S., Head, J. W., Strom, R. G., Chapman, C. R., et al. (2008). Geology of the Caloris basin, Mercury: A view from MESSENGER. *Science*, *321*(5885), 73–76. https://doi.org/10.1126/science.1159261

Namur, O., & Charlier, B. (2017). Silicate mineralogy at the surface of Mercury. *Nature Geoscience*, *10*(1), 9–13. https://doi.org/10.1038/NGEO2860

Naumann, T., & Geist, D. J. (2000). Physical volcanology and structural development of Cerro Azul Volcano, Isabela Island, Galápagos: implications for the development of Galápagos-type shield volcanoes. *Bulletin of Volcanology*, *61*(8), 497–514. https://doi.org/10.1007/s004450050001

Neukum, G., Oberst, J., Hoffmann, H., Wagner, R., & Ivanov, B. A. (2001). Geologic evolution and cratering history of Mercury. *Planetary and Space Science*, *49*(14–15), 1507–1521. https://doi.org/10.1016/S0032-0633(01)00089-7

Ostrach, L. R., Robinson, M. S., Whitten, J. L., Fassett, C. I., Strom, R. G., Head, J. W., & Solomon, S. C. (2015). Extent, age, and resurfacing history of the northern smooth plains on Mercury from MESSENGER observations. *Icarus*, *250*, 602–622. https://doi.org/10.1016/j.icarus.2014.11.010

Peplowski, P. N., Klima, R. L., Lawrence, D. J., Ernst, C. M., Denevi, B. W., Frank, E. A., et al. (2016). Remote sensing evidence for an ancient carbon-bearing crust on Mercury. *Nature Geoscience*, *9*(4), 273–276. https://doi.org/10.1038/ngeo2669

Prockter, L. M., Ernst, C. M., Denevi, B. W., Chapman, C. R., Head, J. W., Fassett, C. I., et al. (2010). Evidence for young volcanism on Mercury from the third MESSENGER flyby. *Science*, *329*(5992), 668–671. https://doi.org/10.1126/science.1188186

Robinson, M. S., Brylow, S. M., Tschimmel, M., Humm, D., Lawrence, S. J., Thomas, P. C., et al. (2010). Lunar Reconnaissance Orbiter Camera (LROC) instrument overview. *Space Science Reviews*, *150*(1–4), 81–124. https://doi.org/10.1007/s11214-010-9634-2

Robinson, M. S., Murchie, S. L., Blewett, D. T., Domingue, D. L., Hawkins, S. E., Head, J. W., et al. (2008). Reflectance and color variations on Mercury: Regolith processes and compositional heterogeneity. *Science*, *321*(5885), 66–69. https://doi.org/10.1126/science.1160080

Rothery, D. A., Mancinelli, P., Guzzetta, L., & Wright, J. (2017). Mercury's Caloris Basin: Continuity between the interior and exterior plains. *Journal of Geophysical Research: Planets*, *122*, 560–576. https://doi.org/10.1002/2017JE005282

Rothery, D. A., Marinangeli, L., Anand, M., Carpenter, J., Christensen, U., Crawford, I. A., et al. (2010). Mercury's surface and composition to be studied by BepiColombo. *Planetary and Space Science*, *58*(1-2), 21–39. https://doi.org/10.1016/j.pss.2008.09.001

Rothery, D. A., Thomas, R. J., & Kerber, L. (2014). Prolonged eruptive history of a compound volcano on Mercury: Volcanic and tectonic implications. *Earth and Planetary Science Letters*, *385*, 59–67. https://doi.org/10.1016/j.epsl.2013.10.023

Sigurdsson, H., Houghton, B. F., McNutt, S. R., Rymer, H., & Stix, J. (2000). *The encyclopedia of volcanoes*. San Diego, CA: Academic Press.

Smith, D. E., Zuber, M. T., Jackson, G. B., Cavanaugh, J. F., Neumann, G. A., Riris, H., et al. (2010). The Lunar Orbiter Laser Altimeter investigation on the Lunar Reconnaissance Orbiter mission. *Space Science Reviews*, *150*(1–4), 209–241. https://doi.org/10.1007/s11214-009-9512-y

Solomon, S. C. (1978). On volcanism and thermal tectonics on one-plate planets. *Geophysical Research Letters*, *5*(6), 461–464. https://doi.org/10.1029/GL005i006p00461

Spudis, P. D., & Guest, J. E. (1988). Stratigraphy and geologic history of Mercury. In *Mercury* (pp. 118–164). Tuscon, AZ: University of Arizona Press

Stockstill-Cahill, K. R., McCoy, T. J., Nittler, L. R., Weider, S. Z., & Hauck, S. A. (2012). Magnesium-rich crustal compositions on Mercury: Implications for magmatism from petrologic modeling. *Journal of Geophysical Research*, *117*, E00L15. https://doi.org/10.1029/2012JE004140

Strom, R. G., Chapman, C. R., Merline, W. J., Solomon, S. C., & Head, J. W. (2008). Mercury cratering record viewed from MESSENGER's first flyby. *Science*, *321*(5885), 79–81. https://doi.org/10.1126/science.1159317

Strom, R. G., & Neukum, G. (1988). The cratering record on Mercury and the origin of impacting objects. In *Mercury* (pp. 336–373). Tuscon, AZ: University of Arizona Press.

Strom, R. G., Trask, N. J., & Guest, J. E. (1975). Tectonism and volcanism on Mercury. *Journal of Geophysical Research*, *80*(17), 2478–2507. https://doi.org/10.1029/JB080i017p02478

Swanson, D. A. (1973). Pahoehoe flows from the 1969-1971 Mauna Ulu eruption, Kilauea volcano, Hawaii. *Bulletin of the Geological Society of America*, *84*(2), 615–626. https://doi.org/10.1130/0016-7606(1973)84<615:PFFTMU>2.0.CO;2

Thomas, R. J., Rothery, D. A., Conway, S. J., & Anand, M. (2014a). Hollows on Mercury: Materials and mechanisms involved in their formation. *Icarus*, *229*, 221–235. https://doi.org/10.1016/j.icarus.2013.11.018

Thomas, R. J., Rothery, D. A., Conway, S. J., & Anand, M. (2014b). Long-lived explosive volcanism on Mercury. *Geophysical Research Letters*, *41*, 6084–6092. https://doi.org/10.1002/2014GL061224

Thomas, R. J., Rothery, D. A., Conway, S. J., & Anand, M. (2014c). Mechanisms of explosive volcanism on Mercury: Implications from its global distribution and morphology. *Journal of Geophysical Research: Planets*, *119*, 2239–2254. https://doi.org/10.1002/2014JE004692

Thomas, R. J., Rothery, D. A., Conway, S. J., & Anand, M. (2015). Explosive volcanism in complex impact craters on Mercury and the Moon: Influence of tectonic regime on depth of magmatic intrusion. *Earth and Planetary Science Letters*, *431*, 164–172. https://doi.org/10.1016/j.epsl.2015.09.029

Thordarson, T., & Larsen, G. (2007). Volcanism in Iceland in historical time: Volcano types, eruption styles and eruptive history. *Journal of Geodynamics*, *43*(1), 118–152. https://doi.org/10.1016/j.jog.2006.09.005

Vaucher, J., Baratoux, D., Toplis, M. J., Pinet, P., Mangold, N., & Kurita, K. (2009). The morphologies of volcanic landforms at Central Elysium Planitia: Evidence for recent and fluid lavas on Mars. *Icarus*, *200*(1), 39–51. https://doi.org/10.1016/j.icarus.2008.11.005

Watters, T. R., Daud, K., Banks, M. E., Selvans, M. M., Chapman, C. R., & Ernst, C. M. (2016). Recent tectonic activity on Mercury revealed by small thrust fault scarps. *Nature Geoscience*, *9*(10), 743–747. https://doi.org/10.1038/ngeo2814

Weider, S. Z., Nittler, L. R., Murchie, S. L., Peplowski, P. N., McCoy, T. J., Kerber, L., et al. (2016). Evidence from MESSENGER for sulfur- and carbon-driven explosive volcanism on Mercury. *Geophysical Research Letters*, *43*, 3653–3661. https://doi.org/10.1002/2016GL068325

Weitz, C. M., & Head, J. W. (1999). Spectral properties of the Marius Hills volcanic complex and implications for the formation of lunar domes and cones. *Journal of Geophysical Research*, *104*(E8), 18,933–18,956. https://doi.org/10.1029/1998JE000630

White, J. D. L., & Ross, P. (2011). Maar-diatreme volcanoes: A review. *Journal of Volcanology and Geothermal Research*, *201*(1–4), 1–29. https://doi.org/10.1016/j.jvolgeores.2011.01.010

Whitten, J. L., Head, J. W., Denevi, B. W., & Solomon, S. C. (2014). Intercrater plains on Mercury: Insights into unit definition, characterization, and origin from MESSENGER datasets. *Icarus*, *241*, 97–113. https://doi.org/10.1016/j.icarus.2014.06.013

Wilson, L., & Head, J. W. (1981). Ascent and eruption of basaltic magma on the Earth and Moon. *Journal of Geophysical Research*, *86*(B4), 2971–3001. https://doi.org/10.1029/JB086iB04p02971

Wilson, L., & Head, J. W. (2008). Volcanism on Mercury: A new model for the history of magma ascent and eruption. *Geophysical Research Letters*, *35*, L23205. https://doi.org/10.1029/2008GL035620

Wöhler, C., Lena, R., Lazzarotti, P., Phillips, J., Wirths, M., Pujic, Z., & Geologic Lunar Research (GLR) Group (2006). A combined spectrophotometric and morphometric study of the lunar mare dome fields near Cauchy, Arago, Hortensius, and Milichius. *Icarus*, *183*(2), 237–264. https://doi.org/10.1016/j.icarus.2006.03.003